

Feed-Forward Inhibition of Androgen Receptor Activity by Glucocorticoid Action in Human Adipocytes

Sean M. Hartig,¹ Bin He,¹ Justin Y. Newberg,¹ Scott A. Ochsner,¹ David S. Loose,³ Rainer B. Lanz,¹ Neil J. McKenna,¹ Benjamin M. Buehrer,⁴ Sean E. McGuire,¹ Marco Marcelli,^{1,2} and Michael A. Mancini^{1,*}

¹Department of Molecular and Cellular Biology

²Michael E. DeBakey VA Medical Center and Department of Medicine
Baylor College of Medicine, Houston, TX 77030, USA

³Department of Integrative Biology and Pharmacology, University of Texas Health Science Center, Houston, TX 77225, USA

⁴Zen-Bio, Inc., Research Triangle Park, NC 27709, USA

*Correspondence: mancini@bcm.edu

<http://dx.doi.org/10.1016/j.chembiol.2012.07.020>

SUMMARY

We compared transcriptomes of terminally differentiated mouse 3T3-L1 and human adipocytes to identify cell-specific differences. Gene expression and high content analysis (HCA) data identified the androgen receptor (AR) as both expressed and functional, exclusively during early human adipocyte differentiation. The AR agonist dihydrotestosterone (DHT) inhibited human adipocyte maturation by downregulation of adipocyte marker genes, but not in 3T3-L1. It is interesting that AR induction corresponded with dexamethasone activation of the glucocorticoid receptor (GR); however, when exposed to the differentiation cocktail required for adipocyte maturation, AR adopted an antagonist conformation and was transcriptionally repressed. To further explore effectors within the cocktail, we applied an image-based support vector machine (SVM) classification scheme to show that adipocyte differentiation components inhibit AR action. The results demonstrate human adipocyte differentiation, via GR activation, upregulates AR but also inhibits AR transcriptional activity.

INTRODUCTION

White adipose tissue is a central metabolic organ that regulates energy balance by storing and mobilizing lipids. In lean individuals, adipocytes maintain a dynamic equilibrium between triglyceride storage and lipolysis. On the other hand, obese subjects have enlarged adipocytes resulting from high caloric intake and increased triglyceride storage in larger lipid droplets. As the obesity epidemic continues to spread, it is likely that a variety of therapeutic intervention strategies will be evaluated, including the targeting of metabolic pathways directly involved in fat synthesis and storage (Guilherme et al., 2008). Thus, the identification of genes associated with human adipocyte differentiation is key to understanding fat deposition and the pathogenesis of obesity.

There is now significant evidence suggesting androgens are important regulators of energy balance, fat deposition, and body composition in males and females (Blouin et al., 2009b), while also influencing other endocrine targets including bone and skeletal muscle (Zitzmann, 2009). It is well established that men experience an increase in body mass index as a consequence of hypogonadism and aging, conditions associated with a decreased level of circulating testosterone (Gould et al., 2007). In women, the association between obesity and androgens is more enigmatic and poorly characterized. Although female androgen receptor (AR) deficiency has not been well studied, women with complete androgen insensitivity syndrome have increased fat mass (Dati et al., 2009). On the other hand, hyperandrogenemia has been known to provoke insulin resistance, independent of obesity (Coviello et al., 2006) through systemic oxidative stress, including disruption of β -cell function (Liu et al., 2010). However, levels of AR do not predict fat distribution or negatively correlate with BMI in men and women (Wake et al., 2007), suggesting that AR activity per se might be differentially regulated in obese versus lean states.

Androgens influence gene transcription through activation of AR, a member of the nuclear receptor (NR) superfamily of transcription factors (Chang et al., 1988; Lubahn et al., 1988). Upon ligand binding, conformational change, and homodimerization, AR can regulate gene transcription by binding to specific DNA motifs (Schoenmakers et al., 2000) that constitute consensus hormone response elements (HREs) in AR target genes. Consensus HREs are also recognized by the glucocorticoid receptor (GR), allowing extensive crosstalk between receptors (Lieberman et al., 1993; Nordeen et al., 1990; Roche et al., 1992) and shared target genes, including the immunophilin *FKBP5* (Magee et al., 2006). Indeed, recent genome-wide analyses have shown that AR and GR binding sites in nonadipocyte cells are enriched in pathways associated with lipid and fatty acid metabolism (Bolton et al., 2007; Massie et al., 2011; Reddy et al., 2009). In 3T3-L1 cells (Yu et al., 2010), primary GR target genes are involved in fatty acid transport (*FABP4*; Hotamisligil et al., 1996), energy storage (*CIDEA*; Nishino et al., 2008), and those that are adipocyte specific (*PPAR γ 2*; Tontonoz et al., 1994). Genome-wide analysis of AR binding in adipocytes has yet to be performed.

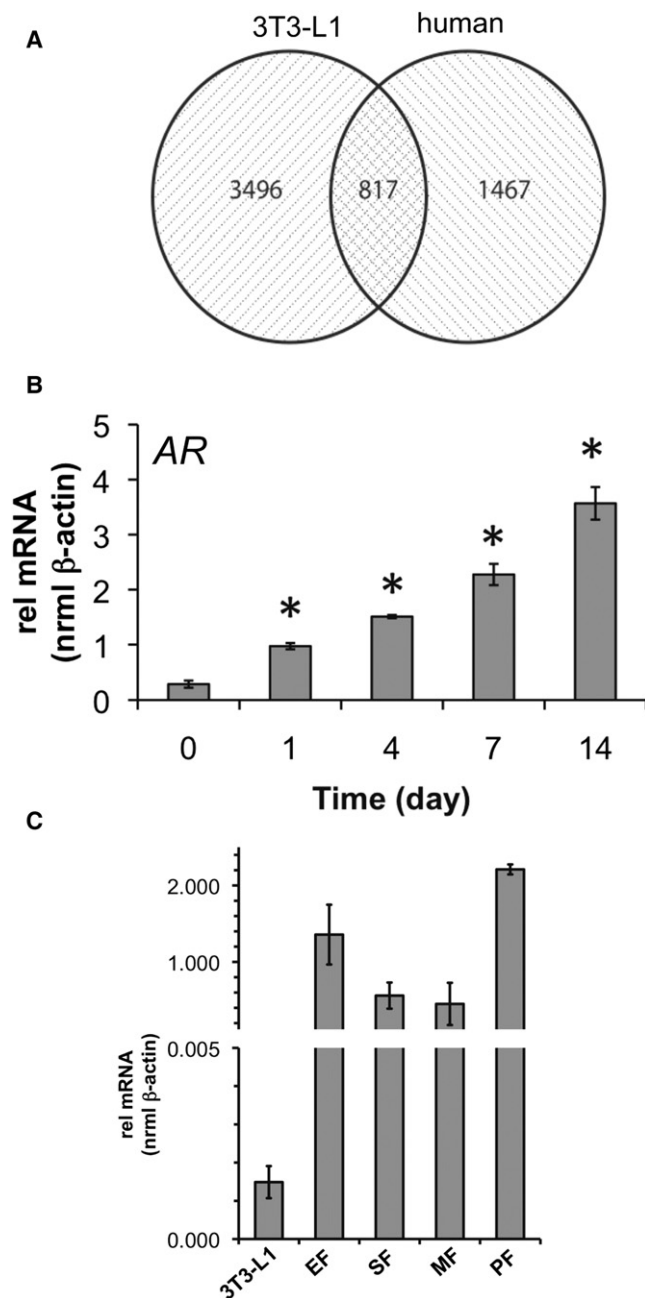


Figure 1. Microarray Analysis Identifies Unique Profiles Associated with Mouse—3T3-L1—and Human Adipocyte Differentiation Models

(A) Comparison of the human expression data to a compatible data set generated in mouse 3T3-L1 found 3,496 and 1,467 genes exclusive to mouse and human microarrays, respectively, with an 817-gene overlap. See also Supplemental Excel File S1.

(B) Of the 1,467 genes regulated in the human class, human *AR* was detected and validated by qPCR (* $p < 0.05$ vs. Day 0).

(C) Expression of *AR* in mouse tissues and cell lines. Total mRNA was isolated, and *AR* transcript levels were compared between epididymal fat (EF), subcutaneous fat (SF), mesenteric fat (MF), peritoneal fat (PF) depots ($n = 3$ mice), and terminally differentiated 3T3-L1 (9 d).

See also Figure S1.

Overall, cell-based studies in human preadipocytes (Blouin et al., 2009a, 2010; Gupta et al., 2008) and 3T3-L1 (Singh et al., 2006) have shown that androgens suppress lipid accumulation during late-stage, terminal endpoints. Here, we have analyzed the transcriptomes of terminally differentiated mouse 3T3-L1 and human adipocytes to identify species-specific genes and pathways involved in the adipogenic process. When we analyzed mRNAs changing during adipogenesis in vitro, we identified an increase in *AR* mRNA specifically in human adipocytes, while it was undetectable in differentiating 3T3-L1 cells. Because the regulation of *AR* and a dominant functional role remains largely undefined, we complemented our transcriptomic discovery with image-based and chemical biology approaches to identify and classify dominant mechanisms of *AR* regulation in adipocytes.

RESULTS

Identification of Genes Unique to Human Adipocyte Differentiation

To identify genes associated with human adipocyte differentiation in vitro, we used Illumina whole genome arrays to measure gene expression in subcutaneous primary human adipocytes treated for up to 14 days with rosiglitazone, 3-isobutyl-1-methylxanthine (IBMX), dexamethasone, and insulin (MIX). An analysis of variance (ANOVA) of gene expression revealed 2674 differentially regulated array features with many of the standard genes associated with adipocyte differentiation up-regulated (Figure S1 available online). Next, we compared gene expression data between terminally differentiated mouse 3T3-L1 adipocytes (Schupp et al., 2009) and human adipocytes differentiated for 14 days. As expected, overlapping probe sets (817; Figure 1A) comprised transcription factors critical for adipocyte differentiation, including *PPAR γ* (Rosen et al., 1999) and *CEBP α* (Rosen et al., 2002), and genes classically associated with cholesterol/fat/lipid metabolism programs, including *ADIPOQ*, *FABP4*, *ABCA1*, *CD36*, and *FASN*, among others (Supplemental Excel File S1). However, we also detected 3,496 and 1,496 genes uniquely expressed in 3T3-L1 (Supplemental Excel File S1) and human (Supplemental Excel File S1) adipocytes, respectively.

Of the genes detected that were changing in the human arrays, *AR* mRNA was upregulated 3.5-fold between Day 0 and Day 14. We validated the induction of *AR* mRNA using quantitative real-time PCR (qPCR) and measured a 3.35-fold induction as early as Day 1, and a 12.3-fold increase over the 14-day differentiation period (Figure 1B). For comparison, we measured *AR* expression in primary mouse adipose tissue. We found *AR* mRNA was expressed in epididymal fat (EF), subcutaneous fat (SF), mesenteric fat (MF), and peritoneal fat (PF) at 910, 376, 302, and 1,484 times the level, respectively, of *AR* expression in mature 3T3-L1 adipocytes (Figure 1C). Our initial findings indicated *AR* was not highly expressed in 3T3-L1 adipocytes.

DHT Inhibits Human Adipocyte Differentiation

Since *AR* mRNA was detected as a significantly expressed and induced gene in human adipocytes, we hypothesized that this differentiation program would be sensitive to androgen (dihydrotestosterone [DHT]) treatment. To test this hypothesis, we applied a set of previously customized image analysis tools

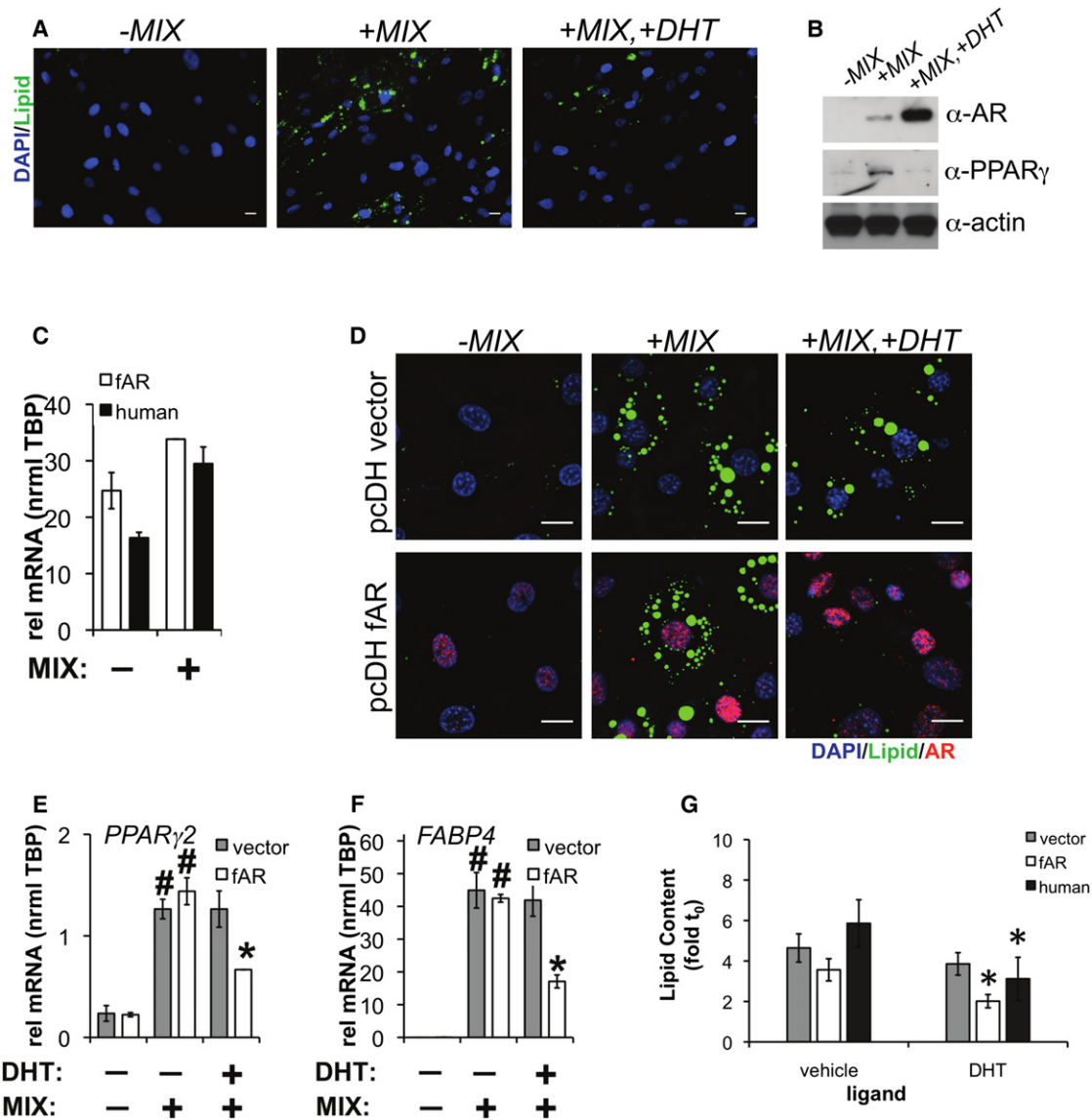


Figure 2. Effect of an Androgen, Dihydrotestosterone, on Adipocyte Differentiation

(A) Human preadipocytes were induced to differentiate for 96 hr with rosiglitazone, insulin, dexamethasone, and IBMX (MIX) in the presence or absence of 10 nM dihydrotestosterone (DHT). Cells were then stained with DAPI (DNA), CellMask Blue (CMBI, general protein dye), and LipidTOX (Lipid), followed by HTM. Scale bar, 20 μ m.

(B) Lysates were prepared from adipocytes differentiated for 4 days in the presence or absence of 10 nM DHT. Protein levels of AR and PPAR γ were detected by western blot.

(C) Human AR-FLAG (fAR) or vector control lentiviral particles were prepared and introduced into 3T3-L1 preadipocytes for 48 hr before chemical induction of differentiation. Human AR expression was detected in both human adipocytes and 3T3L1 expressing fAR before and after 96 hr of differentiation.

(D) After cell differentiation in the presence or absence of 10 nM DHT for 96 hr, cells were processed for immunofluorescence to AR, stained for lipid and DAPI/CMBI, and imaged. Scale bar, 20 μ m.

(E and F) In (E) and (F), PPAR γ 2 and FABP4 mRNA levels, respectively, were measured from 3T3L1 cells expressing vector (pcDH) or fAR differentiated in the presence or absence of 10 nM DHT for 96 hr. (n = 2 independent experiments \pm SEM, #p < 0.05 compared to no differentiation or *p < 0.05 compared to differentiation without DHT).

(G) Lipid accumulation was quantified by HCA after lentiviral expression of human AR (n = average of four wells \pm SEM) or androgen treatment in human preadipocytes (n = five independent experiments \pm SEM, *p < 0.05).

that automatically identify cells and nuclei to extract fluorescence-based measurements (e.g., high content analysis; HCA) of NR and coregulator proteins, and, as a biomarker for differentiation, levels of intracellular lipids (Hartig et al., 2011). As shown

in Figure 2A, MIX-induced adipocyte differentiation was reduced by supplementation with 10 nM DHT at 96 hr as indicated by reduced lipid accumulation. By western blotting, MIX supplemented with 10 nM DHT showed both decreased PPAR γ

expression and increased AR levels (Figure 2B). To further validate the role of AR in adipocyte differentiation, we then compared the effects of DHT on the differentiation of 3T3-L1 adipocytes when human AR was expressed by lentivirus. 3T3-L1 cells were infected with either empty vector (pcDH) or virus encoding human FLAG-AR (pcDH fAR). In response to vehicle (dimethyl sulfoxide; DMSO) or MIX, AR expression in 3T3-L1 was approximately equal to levels found in human adipocytes (Figure 2C). After 48 hr, cells were induced to differentiate with standard 3T3-L1 adipogenic cocktail (dexamethasone, IBMX, insulin) and ethyl alcohol (EtOH) (vehicle), or 10 nM DHT for 96 hr. DHT (10 nM) suppressed lipid accumulation (−44% vs. vehicle) only when AR was expressed by lentivirus and not in the vector control (Figure 2D). The adipocyte-specific genes *PPAR γ 2* (−54% vs. vehicle) (Figure 2E) and *FABP4* (−60% vs. vehicle) (Figure 2F) were also significantly downregulated by DHT only in 3T3-L1 cells expressing human AR. Furthermore, we measured a 47% decrease in lipid accumulation in human adipocytes, which compared well with the effect in 3T3-L1 when AR was expressed by lentivirus (Figure 2G). Our results support previous observations demonstrating inhibition of human adipocyte differentiation by AR agonists (Blouin et al., 2009a, 2010; Gupta et al., 2008). Taken together, we speculated the discrepancy in DHT-mediated inhibition of early adipocyte differentiation between the two cell types is attributable to differences in their AR expression levels. Human adipocytes express sufficient AR at a level where DHT can inhibit early adipogenesis, while extremely low levels of AR in 3T3-L1 cells prohibit any effect of DHT on lipid accumulation.

Human Adipocyte Differentiation Is Suppressed by AR Activation

We next examined the effect of 10 nM DHT and 10 μ M O-hydroxyflutamide (OHF), an AR antagonist, on expression of adipocyte-specific mRNAs and nuclear levels of *PPAR γ* and AR in human subcutaneous preadipocytes induced to differentiate by MIX. Among positive cells, AR and *PPAR γ* exhibited a chiefly nuclear signal (>75%) by immunofluorescence (Figure 3A), which was independent of DHT and OHF. Using AR levels at 96 hr (90th percentile) as a threshold to define AR-positive cells, we established that DHT increased the number of AR positive cells by 3.3-fold compared to MIX (Figure 3B). Of note, the range of expression for positive cells was less than one log between minimum and maximum AR levels. As determined by Pearson's *r* calculation ($N > 3,700$ cells for all treatments), cells exhibiting higher levels of AR as a result of androgen treatment did not correspond with decreased nuclear *PPAR γ* ($Pr_{\text{MIX/DHT}} = 0.105$, $N = 4,765$ cells). Indeed, no treatment induced a significant correlation between nuclear AR and nuclear *PPAR γ* ($Pr_{\text{MIX}} = 0.06$; $Pr_{\text{MIX}} = 0.09$; $Pr_{\text{MIX/OHF}} = 0.05$), suggesting that an upstream regulatory event might contribute to the regulation of both receptors. Following 96 hr of treatment, differentiation of human preadipocytes in the presence of DHT was associated with reduced lipid accumulation (−32%) (Figure 3C), dramatically increased levels of AR protein (10-fold over vehicle) (Figure 3D), and reduced levels of nuclear *PPAR γ* (−20%) (Figure 3E). AR protein stabilization by androgen appears to be the main effect, as AR mRNA levels were only modestly changed during differentiation in the presence of DHT (15% vs. no DHT)

(Figure 3F). Conversely, levels of adipocyte-associated (*C/EBP α* , −79%; *PPAR γ* , −60%) and lipid storage (*ADFP*: −46%, *FASN*: −70%) genes were all reduced under the same conditions (Figure 3F). As a control, the mRNA level of the transcriptional coactivator *SRC-3* was not significantly affected by differentiation in the presence of androgen (DHT) or antiandrogen (OHF). We suggest that AR activation by DHT leads to an accumulation (stabilization) of nuclear AR (Furutani et al., 2002), which reduces expression of *PPAR γ* mRNA and subsequently slows adipocyte differentiation. Collectively, these results extended the findings of Figure 2 and position the activity of AR as a critical determinant of lipid storage in adipocytes.

GR Promotes AR Expression during Human Adipocyte Differentiation

As a pioneer factor in preadipocytes, the GR is required to initiate cell differentiation and activate transcription of proadipocyte genes, including *PPAR γ 2* (Steger et al., 2010). Because recent ChIP-Seq experiments in A549 cells found dexamethasone-induced GR binding regions <10 kB upstream of the AR promoter (Reddy et al., 2009) and AR was significantly upregulated early (~24 hr after differentiation; Figure 2A), we reasoned GR might regulate AR expression. To test this hypothesis, GR was downregulated by siRNA in preadipocytes. Subsequently, cells were treated with MIX or vehicle (EtOH) for 96 hr. Using immunofluorescence (Figure 4A) and HCA, we detected GR knockdown (−54% vs. scR siRNA) (Figure 4B) which corresponded to both decreased lipid accumulation (−35% vs. scR siRNA) (Figure 4C) and reduced nuclear AR (−52% compared to scR siRNA). By qPCR (Figure 4E), GR siRNA inhibited AR mRNA induction with significant downregulation of *PPAR γ 2*, adipogenic targets of *PPAR γ* and GR (*FABP4*, *CIDEA*), and a canonical GR/AR target (*FKBP5*). The marked inhibition of AR induction after GR siRNA suggested GR is required for early upregulation of AR in adipocytes, in addition to the established roles of GR as a primary regulator of early adipogenesis (Pantoja et al., 2008; Steger et al., 2010).

Dexamethasone Is Required for AR Upregulation in Human Adipocytes

To further understand the role of GR and dexamethasone in driving AR upregulation, we examined the uncoupling of dexamethasone (dex) from the three other components (ixr: insulin, IBMX, rosiglitazone) present in MIX. At the mRNA level (Figure 5A), dex supplementation was required for AR induction (4.5-fold vs. EtOH) and maximal upregulation of *PPAR γ 2* (6.4-fold vs. EtOH). Target genes of *PPAR γ 2* and GR, *FABP4*, *CIDEA*, and *FKBP5*, respectively, were each coordinately and significantly upregulated when dex was added to ixr. As observed in Figure 3F, the addition of 10 nM DHT to ixr+dex treatments decreased the expression of *PPAR γ 2* (−58%) and genes associated with lipid transport (*FABP4*: −80%) and storage (*CIDEA*: −60%). Upregulation of *FKBP5* by dex supplementation was unaffected by 10 nM DHT, indicating a dominant effect of dex on target genes shared by both AR and GR.

In parallel experiments, we confirmed the qPCR findings (Figure 5A) and dissected the regulation of AR by dex in human adipocytes using HCA (Figure 5B). Addition of dex to differentiation components (ixr) caused a decrease in GR

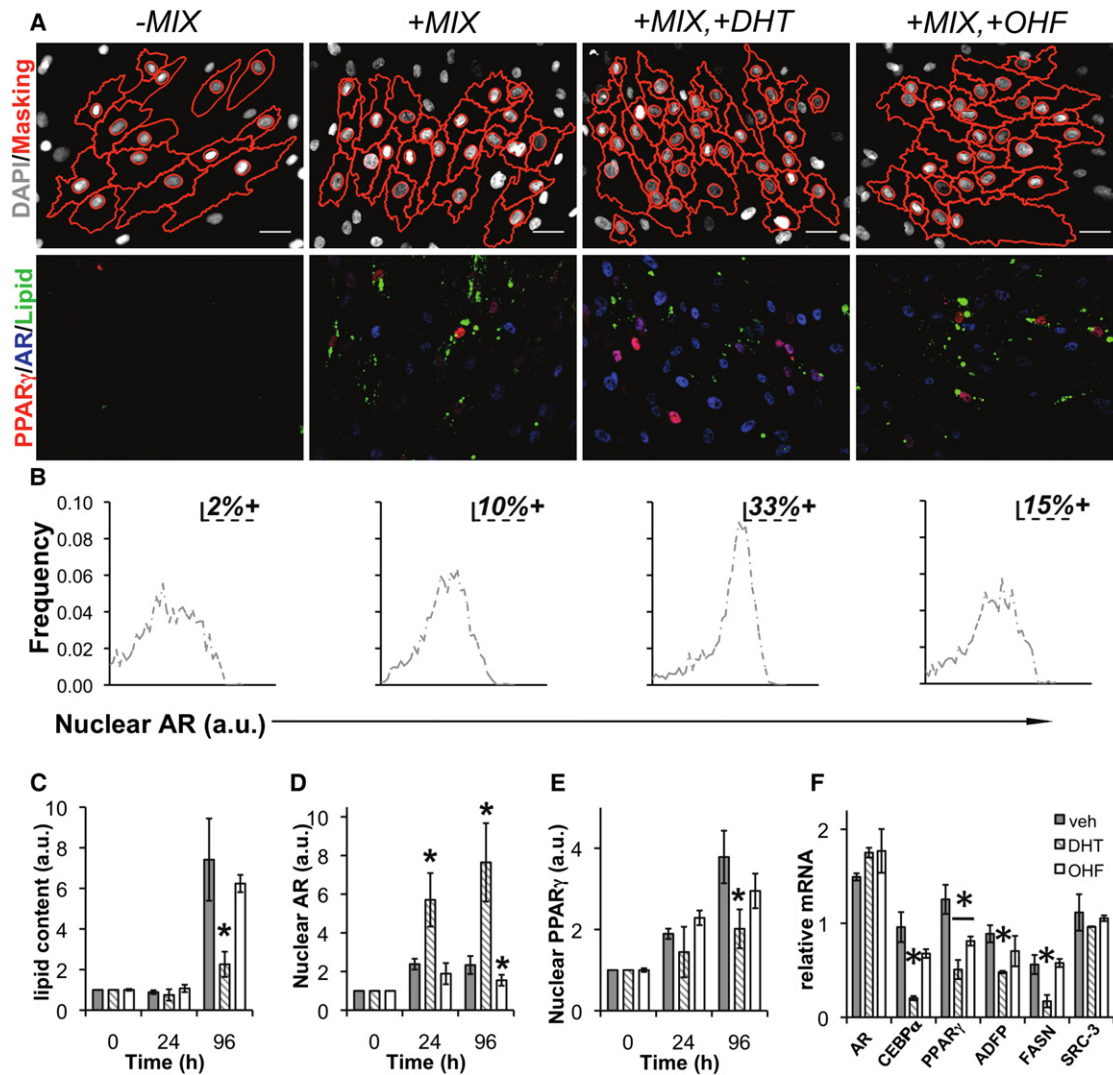


Figure 3. AR Activation Suppresses Human Adipogenesis

(A) Images from human adipocytes differentiated for 96 hr with the indicated ligand treatments, immunolabeled with antibodies to PPAR γ (gray scale) or AR (red), and stained with LipidTOX (Lipid, green), and DAPI. On the leftmost panels, masks (red) generated by image analysis algorithms were overlaid onto the DAPI (gray scale) images to indicate cell and nucleus borders. Scale bar, 50 μ m.

(B) Percent AR-positive cells was defined by measuring the 90th percentile expression level for +MIX and applying that threshold to single cell distributions of AR for the other three treatments. The effect of androgens on the rate of lipid accumulation, nuclear PPAR γ , and nuclear AR was determined by differentiation of human preadipocytes for the indicated time points in the presence of DHT, vehicle (EtOH), or OHF.

(C–F) HCA was used to quantify the induction of (C) lipid accumulation, (D) AR, and (E) PPAR γ . In parallel, relative mRNA was determined for (F) AR, C/EBP α , PPAR γ , ADFP, FASN, and SRC-3.

protein levels (ixr+dex: -21% vs. EtOH) consistent with a ligand- and proteasome-dependent downregulation mechanism (Wallace and Cidlowski, 2001). While the mRNA data indicated that dex was required to upregulate AR mRNA (Figure 5A), DHT addition to any treatment was sufficient to increase AR protein levels with a maximum observed induction of 8.9-fold (ixr+dex+DHT) providing further evidence of androgen-mediated AR stabilization in adipocytes. Collectively, these data show lipid accumulation requires dex, and it is inhibited by supplementation of differentiation cocktail with DHT (ixr+dex+DHT).

Figures 4, 5A, and 5B supported the role of both dex and GR action in driving AR induction in human adipocytes. Although

there was no clear correlation between AR and PPAR γ (Figure 3A), we detected a positive correlation between AR and GR ($r_{\text{MIX}} = 0.57$) as shown in Figure 5C for preadipocytes differentiated (ixr+dex; MIX) for 96 hr. At the single-cell level, we divided the population into low and high GR-expressing cells based on the median level of GR detected after treatment with complete differentiation cocktail (ixr+dex) (Figure 5D). Although median AR levels varied as a function of DHT treatment, temporal analysis of the two subpopulations showed cells with higher GR were associated with both higher lipid (Figure 5E) and AR (Figure 5F) levels. These results suggest that GR (Figure 4) and dex (Figure 5) are needed to regulate AR at the

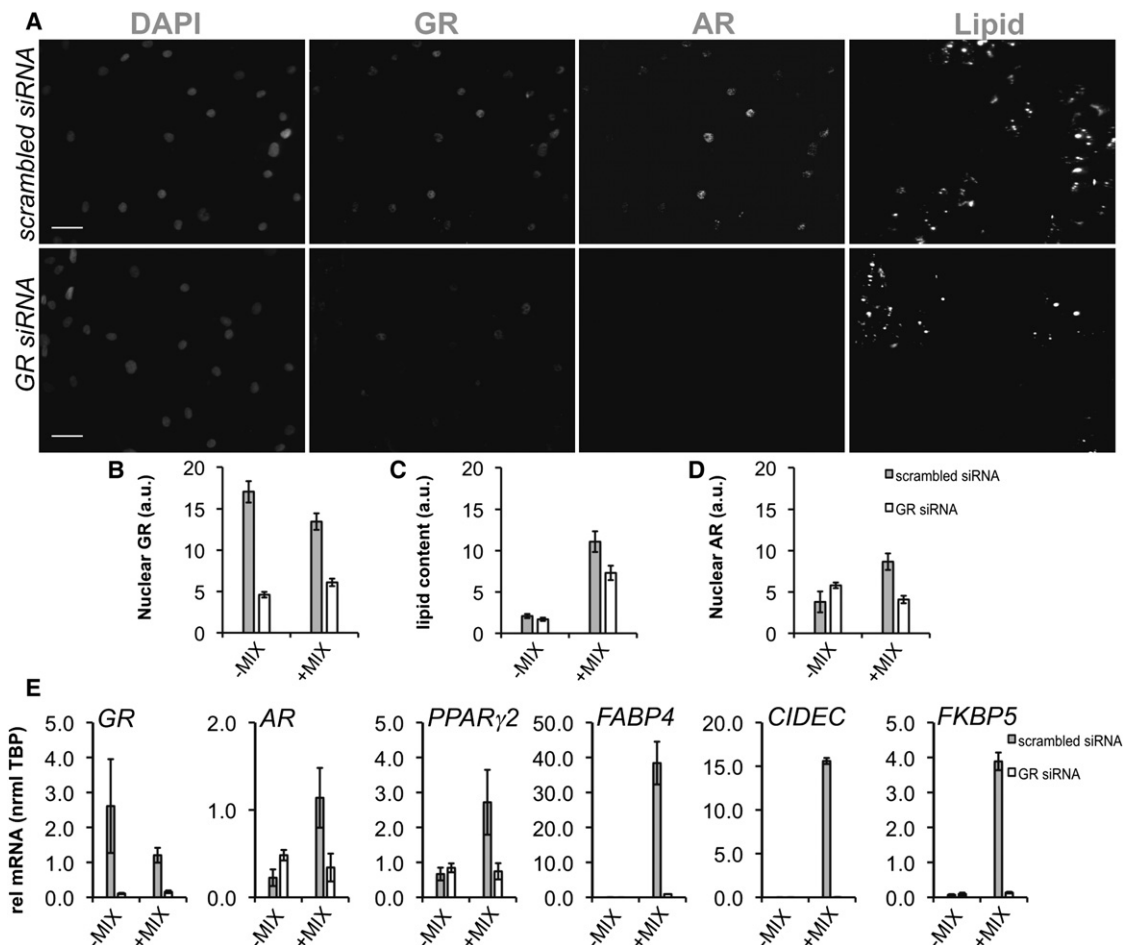


Figure 4. siRNA-Mediated Depletion of GR Inhibits AR Upregulation in Differentiating Human Adipocytes

(A) Preadipocytes were transfected with scrambled (scrambled siRNA) or siRNA to GR (GR siRNA) for 48 hr followed by induction of differentiation (+MIX) and HTM. Scale bar, 50 μ m.

(B–D) HCA detection of (B) nuclear GR, (C) lipid accumulation, and (D) nuclear AR after siRNA transfection ($n \geq 4$ experiments) by immunofluorescence and lipid labeling.

(E) qPCR was used to validate HCA measurements of GR knockdown and downstream effects on AR, lipid accumulation, and target gene expression: *GR*, *AR*, *PPAR γ 2*, *FABP4*, *CIDEA*, and *FKBP5*. RNA was isolated from two independent experiments. Asterisks indicate measured variables statistically different from the nontargeting siRNA control at the 95% confidence level ($*p < 0.05$). Error bars, SEM.

single-cell and transcriptional levels in adipocytes. Although AR expression is increased by dex and GR, we reasoned AR might adopt a repressive conformation that abrogates its ability to prevent adipocyte differentiation.

Adipocyte Differentiation Reagents Modulate AR Conformation

The N-terminal activation function 1 (AF-1) and the C-terminal ligand-dependent (AF-2) domains of AR are largely inactive in the absence of ligand. In the presence of agonists, AR adopts a conformational change allowing communication between AF-1 and AF-2 and subsequent transcriptional activation (Kempainen et al., 1999; Langley et al., 1995; Schaufele et al., 2005). To test our hypothesis regarding inhibition of AR activity, we used a fluorescence resonance energy transfer (FRET)-based assay (Jones et al., 2009; Klock et al., 2007; Schaufele et al., 2005) to determine the effect of differentiation

cocktail on the intramolecular interaction between CFP-AF-1 and YFP-AF-2 domains in full-length AR. In this assay, agonist binding induces a conformational change that brings the cyan fluorescent protein (CFP) and yellow fluorescent protein (YFP) into close proximity, enabling energy transfer, which precedes nuclear translocation and transcriptional activity. In these experiments, we transiently expressed a CFP-AR-YFP fusion protein in HeLa and exposed the cells to 10 nM DHT, EtOH (vehicle), 10 μ M OHF, or MIX for 20 hr (Figure 6A). To detect effects on androgen-induced conformation, OHF/DHT and MIX/DHT treatments were applied. Figure 6B shows that DHT markedly induced nuclear translocation, altered subnuclear localization, and increased energy transfer (7.5-fold), which is indicative of intramolecular events bringing the AF-1 and AF-2 domains into close proximity (Figure 6B). Compared to vehicle, OHF stimulated a lesser increase in FRET (2.4-fold), while MIX showed no significant change. However, treatment

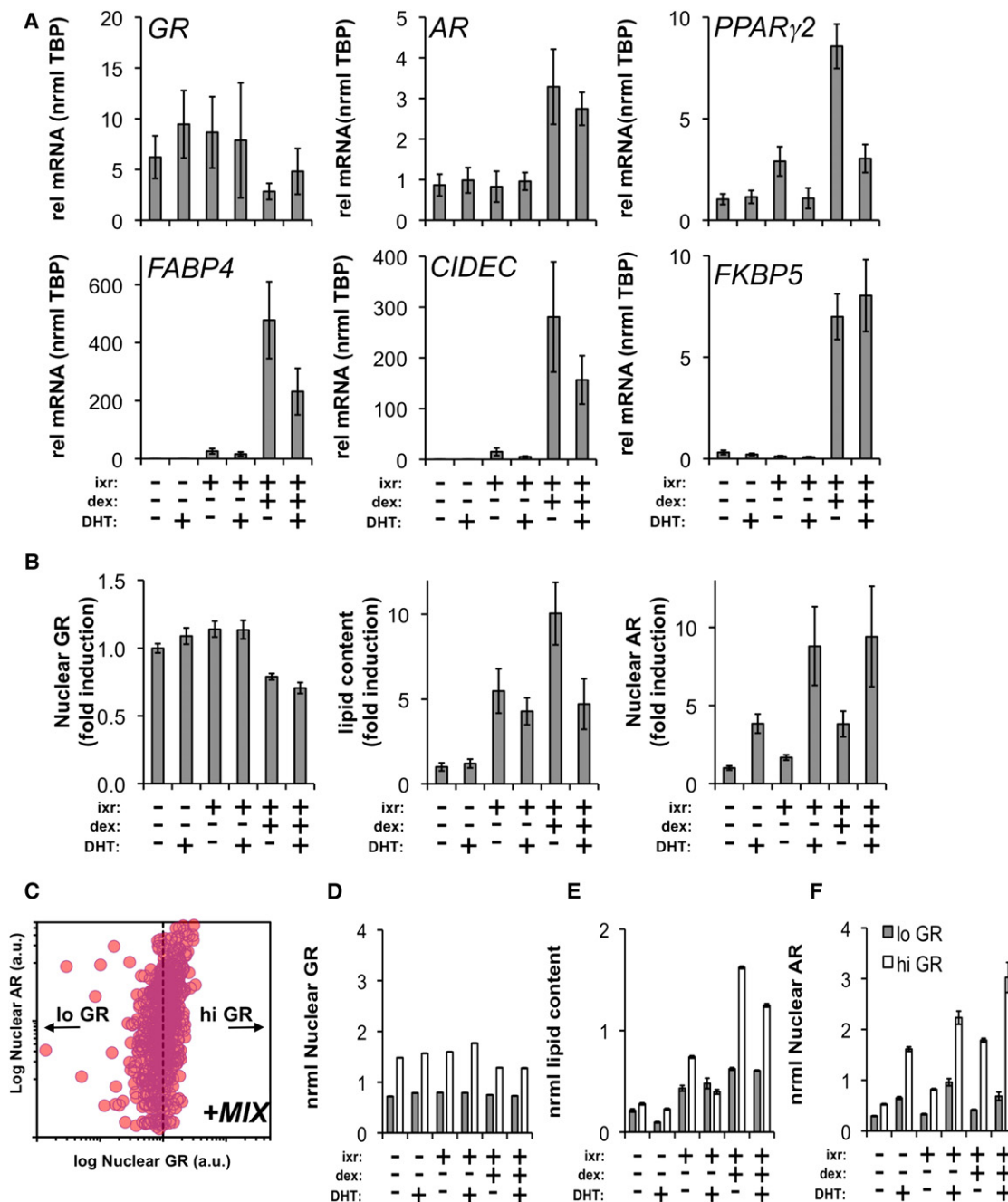


Figure 5. AR Expression Is Correlated with Dexamethasone-Driven Adipocyte Differentiation

(A) Preadipocytes were differentiated (ixr: insulin/IBMX/rosiglitazone) for 96 hr in the presence or absence of dexamethasone (dex) \pm 10 nM DHT. qPCR was used to measure mRNA expression for *GR*, *AR*, *PPAR γ 2*, *FABP4*, *CIDEA*, and *FKBP5*. RNA was isolated from two independent experiments.

(B) In parallel experiments, effects of dex and DHT on AR induction and lipid accumulation were evaluated by HCA. Subsequent to the treatments, GR and AR were detected by immunofluorescence in combination with lipid labeling.

(C) Cell-to-cell correlation between AR and GR was monitored. One representative experiment is shown for cells differentiated with standard cocktail (MIX) for 96 hr. Individual cell measurements of nuclear GR and AR were normalized to the median intensity of standard differentiation cocktail (ixr+dex; MIX) at 96 hr. GR normalization of all treatments set a threshold (dotted line) to subdivide cells into GR^{lo} and GR^{hi} subpopulations.

(D–F) The median single-cell intensities of (D) GR, (E) lipid content, and (F) AR were determined for the GR^{lo} and GR^{hi} populations at 96 hr (* p < 0.05, n \geq 400 cells per treatment). Error bars, SEM.

of cells with OHF or MIX in the presence of 1 nM DHT blocked the androgen-induced conformational change by -43% and -56% , respectively. These experiments suggested that one or more components of adipocyte differentiation cocktail antagonize AR activity by blocking ligand-induced N/C-terminal interactions.

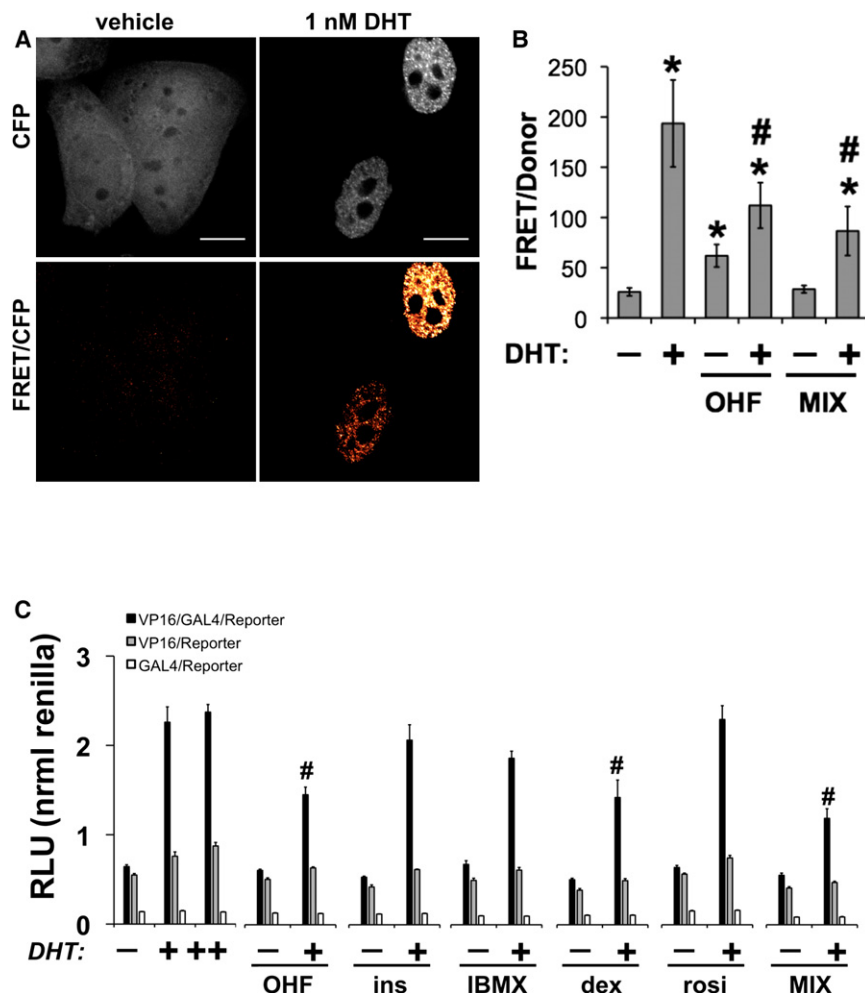


Figure 6. Human Adipocyte Differentiation Alters the Conformation of AR

(A) HeLa cells transiently transfected with GFP-AR-YFP were treated with vehicle, 10 μ M OHF, or differentiation media (MIX) in the presence or absence of 1 nM DHT for 20 hr. Scale bar, 10 μ m. (B) FRET imaging was used to determine AR conformation ($n \geq 10$ cells per condition).

(C) An N-terminal region containing AR 1-660 was fused to the VP16 TAD, while a C-terminal region containing AR 624-919 (wild-type) was fused to the Gal4-DBD domain. HeLa cells were cotransfected with AR fragments and reporter constructs as described in *Experimental Procedures*. After 12 hr of transfection, cells were trypsinized and equally seeded into 96-well plates. Cells were allowed to reattach and subsequently treated with dexamethasone (500 nM), IBMX (250 μ M), insulin (200 nM), rosiglitazone (3 μ M), MIX, and AR ligands, alone or in the presence of 0.1 nM DHT. After 24 hr of treatment, luciferase activity was detected. Data represents the units of firefly luciferase corrected for the units of renilla luciferase detected in the same plate. Shown is one representative experiment from four replications. $p < 0.05$ was considered significant for treatments compared to vehicle (#) or DHT (*) treatments.

In a complementary approach, we used a mammalian two-hybrid assay to determine whether AR N/C-terminal domain interactions might be altered by treatment with each component of the differentiation cocktail. As the agonists bind the ligand-binding domain of AR, the AR (1-660)-VP16 and AR (624-919)-Gal4 fusion proteins become close enough to activate luciferase activity driven by the Gal4-VP16 interaction (Langley et al., 1995). Expression of individual VP16 or Gal4 plasmids were used as negative controls. When we treated cells with individual or all components combined (MIX), the basal AF-1/AF-2 interaction was not affected (Figure 6C). In complementary experiments, we also treated cells with individual or all components (MIX) combined in the presence of 0.1 nM DHT. Similar to OHF, dexamethasone and MIX inhibited DHT-induced N/C-terminal interaction (Figure 6C). Thus, the next step was to determine the extent to which AR transcriptional activity was inhibited by adipocyte differentiation signals.

Inhibition of AR Transcriptional Activity by Chemical Inducers of Adipocyte Differentiation

As MIX components were shown to alter the conformation of AR, we next assessed whether AR translocation and transcriptional activity were similarly modulated. To do this, we created

a transcriptional biosensor cell line based on a parental green fluorescent protein (GFP)-AR HeLa model described previously, which faithfully expresses AR target genes in response to agonist treatments (Szafran et al., 2008). We stably incorporated an ARR_2 PB-dsRED2-skl reporter construct, which is responsive to AR agonists and inhibited by antagonists (in competition experiments), including MIX (Figure 7A).

After image processing, HCA was used to simultaneously quantify GFP-AR subcellular localization (% nuclear AR) (Figure 7B), total AR expression (Figure 7C), and ARR_2 PB-dsRED2-skl reporter activity (Figure 7D) for compound concentrations used in differentiation cocktail. As expected (Szafran et al., 2008), DHT elicited significant, dose-dependent increases in all three features. Dexamethasone, IBMX, and MIX induced AR translocation (Figure 7B), while insulin and MIX upregulated total AR levels (Figure 6C). Although some of the components together (MIX) or individually affected total AR and AR translocation, none increased AR transcriptional activity (Figure 7D). When treatments were performed in the presence of 1 nM DHT (+), several effects were observed. First, insulin, IBMX, and rosiglitazone decreased androgen-induced AR translocation compared to 1 nM DHT (Figure 7B). Second, IBMX, dexamethasone, and rosiglitazone inhibited DHT-induced reporter activity (Figure 7C).

Although our three basic measurements reporting important mechanisms of AR activity were informative (Figures 7B–7D), they do not encompass the wealth of phenotypic data available in the images, which can characterize the biological phenotypes caused by the different compound treatments. Extending

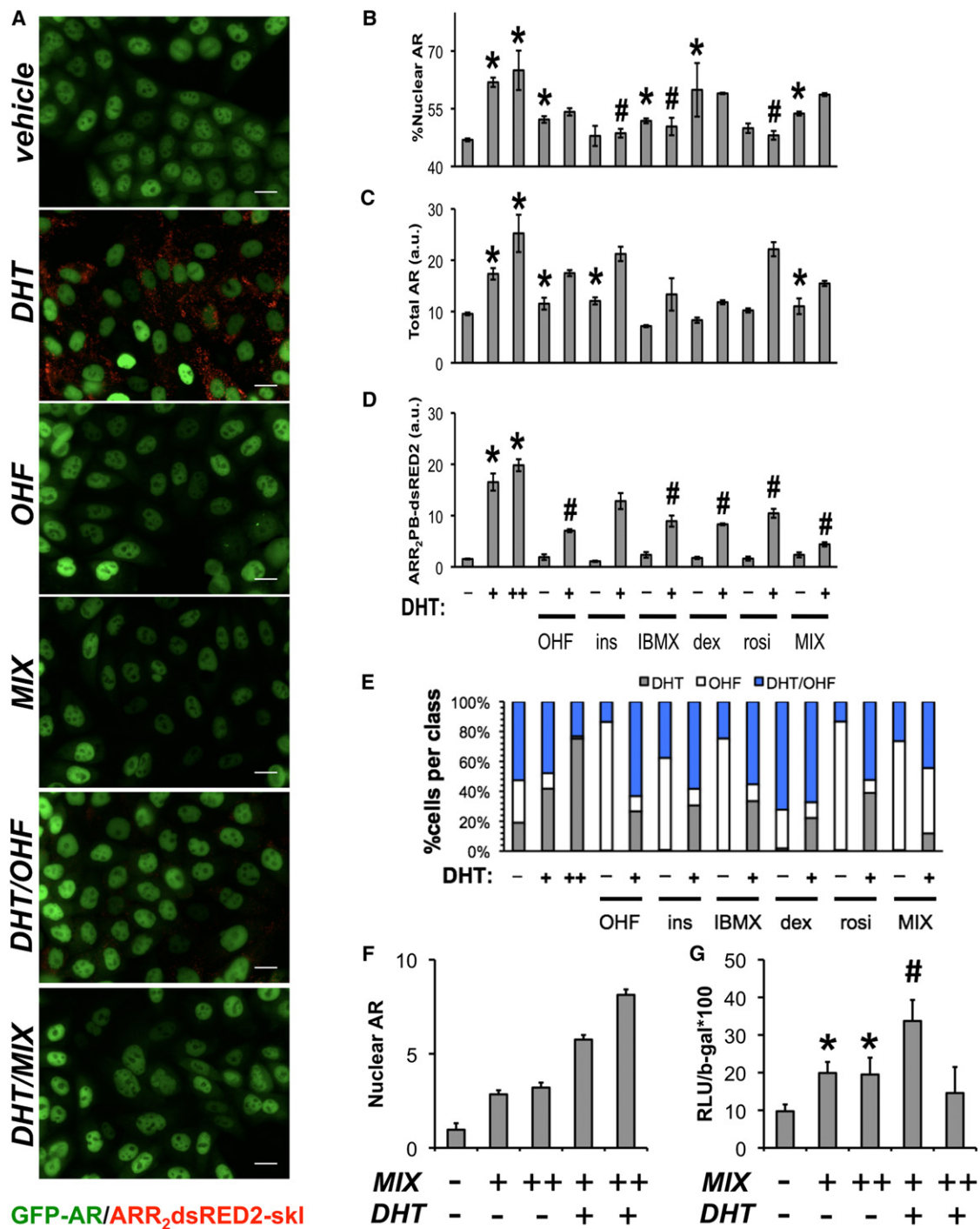


Figure 7. Adipocyte Differentiation Reagents Repress AR Transcriptional Activity

(A–D) GFP-AR:ARR₂PB-dsRED2-skl double-stable HeLa cells were used to evaluate effects of differentiation reagents (~48 hr) on GFP AR nuclear translocation, total AR levels, and androgen-dependent reporter activity encoded by the expression of peroxisome-targeted dsRED2. After treatment, experiments were processed for automated microscopy, imaged, and segmented into single-cell regions for feature extraction (A). Response data are depicted for (B) nuclear translocation, (C) total AR, and (D) ARR₂PB-dsRED2-skl activity for the indicated treatments. Experiments were performed in the presence and absence of 1 nM DHT. One representative experiment from three replications is shown; $p < 0.05$ was considered significant for treatments compared to vehicle (#) or DHT (*) treatments.

(E and F) In (E), SVM allowed more sensitive detection of AR repression by adipocyte differentiation components. An SVM classifier was trained to recognize OHF, DHT, or DHT/OHF patterns and applied to cell-level responses (from the DAPI, GFP-AR, and ARR₂PB-dsRED2-skl channels). Cells were automatically classified into DHT, OHF, or DHT/OHF treatment groups based on selected, robust subcellular measurements used by the SVM classifier. For each subplot, the abscissa represents compound treatments, while the ordinate denotes the percentage of cells assigned to each population. To validate effects on AR-mediated

our recently developed HCA approaches designed to classify estrogen receptor responses (Ashcroft et al., 2011), we identified single-cell-level features that classified MIX components based on their similarity to control treatments. We generated a control data set consisting of cells treated with 10 nM DHT, 10 μ M OHF, or 1 nM DHT + 10 μ M OHF. After image processing, we extracted intensity- and morphology-based features (276 measurements per cell) from the GFP-AR and ARR₂PB-dsRED2-skl channels. These measurements include mechanistic features (e.g., GFP-AR levels and localization), cytological features (e.g., GFP-AR nuclear variance (Szafran et al., 2008)) and statistical features (e.g., cytoplasmic ARR₂PB-dsRED2-skl kurtosis). We processed the features and applied stepwise discriminant analysis (Jennrich, 1977), which selected 32 features especially useful in distinguishing between control treatments (Table S1). Finally, we trained a classifier on the control data using the SDA-selected features, which was used to classify the cells from the compound treatments. This classification framework was validated on the control data to assess classifier performance (Table S1). From classification, we were able to identify the percentage of cells exhibiting AR agonism or antagonism given a particular treatment (Figure 7E). It is interesting that, by incorporating effects on GFP-AR protein levels, localization, subnuclear pattern, and reporter levels, this approach had high enough sensitivity to detect effects of all MIX components in the absence of DHT, which was impossible by CFP-AR-YFP (Figure 6B) or mammalian two-hybrid assays (Figure 6C).

Figure 7E suggested that each MIX compound redistributed cell populations to predominantly OHF or DHT/OHF phenotypes. Also, during DHT treatment, individual addition of IBMX, insulin, or rosiglitazone decreased the number of cells classified as agonist (DHT) and increased the number of cells classified as antiandrogen (DHT/OHF). Furthermore, MIX reflected the individual components and was classified as a predominantly antagonist treatment (e.g., OHF alone or DHT/OHF) with a complete loss of the DHT class.

To complement our findings in the GFP-AR:ARR₂PB-dsRED2 biosensor cell line and verify the inhibition of AR transcriptional activity by adipocyte differentiation reagents, we expressed the AR-specific ARR₂PB-luciferase reporter plasmid (Schoenmakers et al., 2000) in terminally differentiated human adipocytes. We found nuclear AR was increased by 2.84-fold in cells differentiated for 7 days (MIX, +; DHT, -), while not significantly increased compared to 96 hr (Figure 3D). Treatment with MIX for 2 additional days (MIX, ++; DHT, -) did not significantly increase nuclear AR. An additional 2 days of treatments with androgen alone (MIX, +; DHT, +), or androgen and MIX (DHT, +; MIX, ++), resulted increased nuclear AR 5.8-fold and 8.1-fold compared to vehicle treatment (MIX, -; DHT, -), respectively (Figure 7F). Concomitantly, when ARR₂PB-luciferase was expressed in terminally differentiated adipocytes (7 days), androgen-induced transcriptional activity was decreased when cells were treated with both DHT and MIX for an additional 2 days (Figure 7G).

These combined experimental approaches show that, in human preadipocytes, AR is upregulated by dexamethasone activation of GR, while also transcriptionally inhibited to putatively promote features of adipocyte maturation.

DISCUSSION

The identification of modulators of human adipocyte gene expression is central to understanding the mechanisms of obesity. Our comparative analysis of the transcriptomes from differentiated human adipocytes and terminally differentiated mouse 3T3-L1 adipocytes (Schupp et al., 2009) suggested that early, significant AR upregulation and function is a specific feature of the human preadipocyte differentiation model (Figure 1). Recently, AR was reported to be expressed at low (Fu et al., 2005) or undetectable (Lahnalampi et al., 2010) levels in 3T3-L1 cells. In our experiments, DHT only inhibited mouse 3T3-L1 differentiation when AR was exogenously expressed by lentivirus, whereas lipid accumulation was clearly reduced in human adipocytes 4 days postinduction (Figure 2). Inhibition of human adipocyte differentiation by DHT was further marked by parallel increases in AR protein levels and repression of adipocyte-specific markers (Figure 3) at the protein (PPAR γ) and gene (*FASN*, *PPAR γ* , *ADFP*, and *C/EBP α*) levels. Indeed, consistent with our effects of DHT on lipid accumulation, DHT has also been found to reduce expression of ACC1 and DGAT2, key enzymes in triacylglycerol synthesis (Gupta et al., 2008).

Upon ligand binding and conformational change, AR, progesterone receptor (PR), mineralocorticoid receptor (MR), and GR can regulate gene transcription by binding a consensus GGT/AACAnnnTGTTCT hormone response element (HRE) (Lieberman et al., 1993; Lombès et al., 1993; Nordeen et al., 1990; Roche et al., 1992). Due to the shared consensus binding motifs for AR, GR, MR, and PR, these receptors can affect the transcriptional activity and regulation of other Type 1 members. For example, both PR and AR have been shown to inhibit GR transcriptional activity at HREs (Archer et al., 1994; Chen et al., 1997; Yen et al., 1997). Therefore, the common DNA-binding site that AR, MR, PR, and GR share provides a capacity to mediate cellular responses through intrareceptor crosstalk. Specifically, recent work has shown that dexamethasone induces GR binding upstream of AR (Reddy et al., 2009). We therefore propose that dexamethasone mobilizes GR to launch adipocyte differentiation, positioning GR as a central regulator of early differentiation and AR expression. Our work shows that GR (Figure 4), regulated by dexamethasone (Figure 5), is required to induce AR expression and regulate the adipocyte phenotype. Novel to the understanding of the GR/AR interrelated gene network, we also established nuclear GR levels are tightly correlated with lipid accumulation (Figure 5D) and nuclear AR (Figure 5E) at the single-cell level during differentiation.

We sought to identify further elements of the AR regulation circuit by analyzing effects of adipocyte differentiation

transcription in primary cells, human preadipocytes were differentiated (MIX) for 7 days followed by transfection of cells with pARR₂PB-luciferase and β -galactosidase (β -gal). Subsequently, cells were treated with 10 nM DHT alone or MIX \pm 10 nM DHT for 48 hr in serum-containing media. Effects of these treatments on (F) AR levels were evaluated by HCA ($n \geq 100$ cells per condition).

(G) ARR₂PB luciferase activity was measured and normalized to β -gal ($n = 3 \pm$ SEM). Scale bar, 20 μ m.

See also Table S1.

conditions on AR conformation and transcriptional activity. First, adipocyte differentiation reagents reduce androgen-dependent AR N/C-terminal interactions (Figures 6A and 6B), inducing quantitatively similar results as a classic antiandrogen (OHF). Second, we used a novel AR fluorescent biosensor cell line and HCA to identify how individual components of adipocyte differentiation cocktail antagonize AR activity and affect transcriptional competence (Figures 7A–7E). Coupled with a machine-learning algorithm to classify subtle phenotypes into DHT, OHF, and DHT/OHF treatments, we were able to establish rosiglitazone and dexamethasone as potent inhibitors of AR activity. Androgen-regulated AR transcriptional activity in human adipocytes was decreased by differentiation cocktail (Figure 7G), which validated our findings in GFP-AR:ARR2PB-dsRED2 biosensor cells. Previous studies have shown dexamethasone and glucocorticoids can inhibit androgen action and downregulate AR activity by competing for androgen response elements (Burnstein et al., 1995; Davies and Rushmere, 1990) without high affinity binding to AR (Wilson and French, 1976). Rosiglitazone, on the other hand, suppresses AR-regulated genes, including the ARR2PB composite reporter, by reduction of agonist-induced receptor binding to DNA (Moss et al., 2010; Yang et al., 2006).

Clinical and epidemiological data imply the existence of a negative cycle between circulating testosterone and obesity, although AR mRNA is unaltered with increasing BMI, independent of sex (Wake et al., 2007). Indeed, further supporting inhibition of AR transcriptional activity during fat maturation, each MIX component has been shown to induce adipogenesis in vivo (De Vos et al., 1996; Fujikura et al., 2005; Madsen et al., 2008; Masuzaki et al., 2001, 2003). Furthermore, testosterone production is suppressed by visceral obesity (Stanworth and Jones, 2009), and patients with visceral obesity and the metabolic syndrome have higher incidence of hypogonadism (Gould et al., 2007).

Androgens have been thought to block adipocyte differentiation (Blouin et al., 2009a, 2010; Gupta et al., 2008; Singh et al., 2003, 2006) by upregulation of Wnt target genes (Singh et al., 2006). In our transcriptome analysis, we detected 51 Wnt target genes exhibiting at least 2-fold change (Supplemental Excel File S1), including targets upregulated by testosterone (*CD44*, *FST*, *LEF1*). Ninety-two percent of the Wnt target genes were downregulated between preadipocyte and terminal differentiation, which may correspond to decreased AR activity. PPAR γ (Liu and Farmer, 2004; Waki et al., 2007) and GR (Bujalska et al., 2006) activation repress Wnt target genes. Thus, subtle alterations in the activity of proadipogenic transcription factors may sustain repression of Wnt signaling via inhibition of AR.

Recent studies (Veilleux et al., 2012) support our findings by showing androgens and glucocorticoids exhibit extensive crosstalk to direct lipid storage in a sex- and depot-specific manner by increasing androgen metabolism. Although excess glucocorticoids and androgens can profoundly affect adipocyte function and promote altered metabolism, additional studies are required to better understand how selective manipulation of the AR/GR axis controls fat deposition and improves overall lipid profiles. Finally, the experiments described in this article propose a feed-forward loop whereby glucocorticoids activate GR to promote AR expression yet inhibit AR activity. Because

peripheral fat tissue contains the enzymatic machinery to synthesize GR agonists, it is possible that these steroids produced in loco are responsible for AR antagonism and activation of lipid storage genes that contributes to maintenance of proper energy balance (Lee et al., 2008).

SIGNIFICANCE

The characterization of genes associated with human adipocytes is fundamental to understanding the pathogenesis of obesity. Given this need, we identified specific genes associated with the primary, early human adipocyte differentiation program that are not sufficiently expressed in 3T3-L1. In support of recent epigenomic analyses of mouse 3T3-L1 and human adipocyte systems (Mikkelsen et al., 2010; Soccio et al., 2011), the 3T3-L1 and human adipocyte transcriptomes are also dissimilar. In this study, we used high content analysis and quantitative imaging to show that in vitro human adipocytes express AR mRNA and protein, regulated by both GR and dexamethasone action, and GR and AR levels are directly correlated. Of specific importance, we used novel image analysis tools to establish antagonism of AR by adipocyte differentiation components, and identified dexamethasone as the dominant inhibitor of AR transcriptional activity. AR mRNA is not negatively correlated with body mass index (Wake et al., 2007), suggesting that obesity does not downregulate AR but negatively modulates its activity. Our data suggest that GR and corticosteroids can both positively regulate AR expression while simultaneously decreasing AR activity and alter androgen effects on energy storage. Since androgens favorably direct muscle differentiation (Singh et al., 2003), regulate muscle mass (Chambon et al., 2010), and increase lean body mass in aging males (Tenover, 1992) and females (Rariy et al., 2011), the use of selective GR or AR modulators in combination may play a role in alleviating the consequences of obesity.

EXPERIMENTAL PROCEDURES

Primary Cell Culture and Differentiation

Cryopreserved, subcutaneous primary human preadipocytes from normal female donors with an average body mass index of 27.51 were provided by Zen-Bio Inc. (Research Triangle Park, NC, USA). Cells were received at passage 2, and experiments were performed before passage 10. Experiments were performed using pooled human preadipocytes from five individual female donors (Lot SL0033). Both human preadipocytes and 3T3-L1 cells were maintained at 5% CO₂/37°C in Dulbecco's modified Eagle medium (DMEM)/F12 (Mediatech, Manassas, VA, USA) with 10% fetal bovine serum (FBS; Gemini Bio-Products, West Sacramento, CA), 100 U/ml penicillin, 100 μ g/ml streptomycin (growth media). Medium was replaced during routine maintenance every 2 days.

Confluent cells were differentiated using growth media supplemented with 100 nM human insulin, 0.250 mM 3-isobutyl-1-methylxanthine (IBMX), 500 nM dexamethasone, and 3 μ M rosiglitazone (BRL49653, Cayman Chemical Company, Ann Arbor, MI, USA). IBMX, insulin, and dexamethasone were purchased from Sigma Chemical Company (St. Louis, MO, USA).

DNA Microarrays

Microarray analysis was performed using the Illumina Sentrix Beadchip Array (Human HT-12) containing ~48,000 probe sequences that spans the human transcriptome. Adipocytes were differentiated for the indicated periods and washed, and total RNA was prepared using RNeasy (QIAGEN, Valencia, CA,

USA). RNA was purified on a QIAGEN Mini spin column. Two hundred nanograms of total RNA were amplified and purified using Illumina TotalPrep RNA Amplification Kit (Ambion, Catalog # IL1791) following the manufacturer's instructions. The first strand of cDNA was synthesized by incubating RNA with T7 oligo(dT) primer and reverse transcriptase mix at 42°C for 2 hr. RNase H and DNA polymerase master mix were immediately added into the reaction mix following reverse transcription and were incubated for 2 hr at 16°C to synthesize second strand cDNA. In vitro transcription was performed and biotinylated cRNA was synthesized by a 16 hr amplification with dNTP mix containing biotin-dUTP and T7 RNA polymerase. Amplified cRNA was subsequently purified, and the concentration was measured by NanoDrop ND-1000 Spectrophotometer (NanoDrop Technologies, Wilmington, DE, USA). An aliquot of 1.5 µg of amplified products was loaded on to Illumina Human HT-12 Beadchips and hybridized at 58°C for 17 hr, washed, and incubated with streptavidin-Cy3 to detect biotin-labeled cRNA on the arrays. Arrays were dried and scanned using a BeadArray Reader (Illumina, San Diego, CA, USA). Each microarray was performed, minimally, with three independent RNA isolates. We performed microarrays at 7 time points: Day 0 (n = 5), Day 1 (n = 4), Day 2 (n = 4), Day 3 (n = 4), Day 4 (n = 4), Day 7 (n = 3), and Day 14 (n = 4).

Microarray Analysis

Background subtracted and quantile normalized gene expression values were calculated using Illumina BeadStudio Software. Differential gene expression was calculated by fitting a linear model to a group means parameterization coupled to a secondary fit of all possible pairwise comparisons equating to an ANOVA using R2.10 and the Limma 2.19 analysis package. Controlling the false discovery rate (FDR) was used to correct for multiple testing. Genes presented in the heatmap are transcripts with a minimum 4-fold change at any given contrast (FDR $q < 0.0001$). Samples were clustered using complete agglomeration and Euclidean distance. Rows were scaled to have a mean of 0 and SD of 1. 3T3-L1 gene expression data was obtained from GSE14004 (Schupp et al., 2009).

RNA Extraction and qPCR Analysis

Total RNA was extracted from cells using the RNeasy kit (QIAGEN, Germantown, MD, USA), following the manufacturer's instructions. To measure relative mRNA expression, qPCR was performed using the Taqman RT-PCR one-step master mix in conjunction with an ABI 7500 real-time PCR system (Applied Biosystems, Foster City, CA, USA). Each sample was tested in duplicate in two independent experiments. β -actin and TATA box-binding protein were used as invariant controls. TaqMan Gene Expression Assays were used for the following human genes: CEBP α , Assay ID Hs00269972_s1; PPAR γ 2, Assay ID Hs01115513_m1; GR, Assay ID Hs00353740_m1; CIDEA, Assay ID Hs01032998_m1; FABP4, Assay ID Hs01086177_m1; FKBP5, Assay ID Hs01561006_m1; AR, Assay ID Hs00171172_m1. The following primer and probe sets were used to detect human (h) hFASN, hSRC-3, and hADFP. hFASN: cggagtgatctgggtgat(F), caggcacacacgatggac(R), Roche Universal Probe Library probe #11 (probe); hSRC-3: ggacctgtaagaaggtgtattcag (F), tgaccttagcataggacacaga (R), tccatgcgcagcatgaaggaga (probe); hADFP: gtgactggcagtggtgagaag (F), tccgactcccaagactgt (R), ccaagtctgtgctgctggcagca (probe). Murine FABP4 and PPAR γ 2 were detected with the following primer and probe sets: mPPAR γ 2: gaaagacaacggacaataacc (F), gggggtgatgtttgactgt (R), Roche Universal Probe Library probe #7 (probe); mFABP4: aagagaaaacgagatggtgacaa (F), cttgtggaagtcacgccttt (L), Roche Universal Probe Library probe #31 (probe).

siRNA Transfection

Before cell plating, optical quality 96-well plates (Greiner Sensoplate Plus, Monroe, NC, USA) were coated with 50 µl of FBS (Gemini Bio-Products) overnight at 37°C. Confluent preadipocytes were transfected with GR siRNA (QIAGEN, Germantown, MD, USA) or mismatch control at a final concentration of 20 nM using Dharmafect transfection reagent (Dharmacon, Lafayette, CO, USA). After transfection, cells were incubated for 48 hr at 5% CO₂/37°C before induction of differentiation for 96 hr.

Antibodies

The following antibodies were purchased from commercial sources and used for immunofluorescence and western blotting: rabbit polyclonal AR (N-20, Santa

Cruz Biotechnology, Santa Cruz, CA, USA), rabbit monoclonal PPAR γ (Cell Signaling, Danvers, MA, USA), GR (Genetex, Irvine, CA, USA), and mouse monoclonal PPAR γ (clone E-8, Santa Cruz Biotechnology, Santa Cruz, CA, USA). Mouse monoclonal antibody to AR (AR-441) (Nazareth et al., 1999) was kindly provided by Dean Edward and Nancy Weigel (Baylor College of Medicine, Houston, TX, USA).

Western Blotting

Cells were collected by scraping, and lysed in RIPA buffer supplemented with the appropriate proteinase and phosphatase inhibitors. Protein concentration was standardized by BCA assay. Western blot analysis was performed with whole cell lysates run on 4%–12% Bis-Tris NuPage (Millipore, Bedford, MA, USA) gels and transferred onto Immobilon-P Transfer Membranes (Millipore). Membranes were blocked 1 hr with 5% milk (in Tris-buffered saline [TBS] with 0.1% Tween-20). Primary antibodies were incubated overnight at 4°C, followed by secondary antibodies for 1 hr at room temperature. Immunoreactive bands were visualized by SuperSignal West Femto chemiluminescence reagents (Pierce, Rockford, IL, USA). All membranes were then subjected to stripping buffer (Pierce) for 30 min at room temperature, reblocked, and probed for β -actin (mouse monoclonal, Sigma Chemical Co.) as a loading control.

Immunofluorescence

For fluorescence detection of antibodies and neutral lipid content in multiwell plates, the following protocol was carried out on the BioMek NX (Beckman Coulter, Fullerton, CA, USA). Well plate systems used were: 96-well and 384-well (Greiner Sensoplate Plus, Monroe, NC, USA). Aspirations and plate washes were performed with an ELx405 (BioTek, Winooski, VT, USA). After differentiation, media was aspirated and 4% formaldehyde (sold as ultrapure paraformaldehyde, Electron Microscopy Sciences, Hatfield, PA, USA) in PBS was immediately added for 30 min at room temperature. Plates were then quenched with 100 mM ammonium chloride. After quenching, plates were washed three times with TBS. Fixed adipocytes were permeabilized with 0.1% Triton X-100 in TBS for 10 min and washed three times with TBS. Nonspecific antibody binding was blocked by preincubating for 30 min in 2% bovine serum albumin in TBS/0.01% saponin (which was also used as an antibody diluent) at room temperature. Antibodies were then diluted at a 1:200 concentration in antibody diluent and incubated overnight at 4°C. Subsequently, plates were washed with TBS and incubated with secondary antibodies for 1 hr at room temperature. AlexaFluor 647-conjugated antimouse and AlexaFluor 568-conjugated antirabbit secondary antibodies (Molecular Probes, Invitrogen) were used. Cells were then washed three times and incubated with CellMask Blue (1 µg/ml, Invitrogen, a general protein dye), LipidTOX green (1:1,000, Invitrogen, a nonpolar lipid-binding dye), and DAPI (10 µg/ml, a DNA-specific dye) in PBS for 45 min at room temperature. Dyes were then aspirated, PBS/0.01% azide was added, and plates were imaged immediately.

Imaging and Microscopy

For high-speed image acquisition for subsequent analysis, cells were imaged using the Cell Lab IC-100 Image Cytometer (IC-100; Beckman Coulter) equipped with a Nikon S Fluor 20 \times /0.75NA objective. The imaging camera (Hamamatsu; Bridgewater, NJ, USA) was set to capture eight bit images at 2 \times 2 binning (672 \times 512 pixels, 0.684 \times 0.684 µm²/pixel) with five images captured per field (DAPI, CMBI, LipidTOX, A568 and A647 secondary antibodies). In general, 12–16 images were captured per well for image analysis. Experiments performed in stable HeLa cell lines and 3T3-L1 were imaged with a 40 \times /0.90NA objective.

Image Processing

Images were analyzed using custom algorithms developed with the Pipeline Pilot (v7.5) software platform (Accelrys; San Diego, CA, USA) in a similar workflow as previously described (Hartig et al., 2011; Szafran et al., 2008). After background subtraction, nuclear and cell masks are generated using a combination of nonlinear least-squares and watershed-from-markers image manipulations of the DAPI images. Cell populations were filtered to discard events with cell aggregates, mitotic cells, apoptotic cells, cellular debris, or poor segmentation. Applied gates were based upon nuclear area, nuclear

circularity, and cell size/nucleus ratio. In general, these filters removed 10% of the population of segmented cells. All events with whole cell masks bordering the edge of the image were additionally eliminated from analysis. Postanalysis measurements were exported to spreadsheet software (Microsoft Excel) for further analysis.

Production of Lentiviral Particles

Human AR cDNA was cloned into the lentiviral expression vector pCDH-CMV-MCS-EF1-Puro (System Biosciences, Mountain View, CA, USA) by Xba I/Nhe I digestion. Pseudolentiviruses were produced in 293TN cells by cotransfecting lentiviral expression constructs and the pPACK packaging plasmid mix (System Biosciences). Pseudoviral particles were harvested 48 hr posttransfection and were concentrated using PEG-it virus precipitation solution kit (System Biosciences).

FRET Imaging

CFP/YFP FRET experiments were performed using a CFP-AR-YFP construct and reagents kindly provided by Fred Schaufele (University of California, San Francisco) and Fahri Saatcioglu (University of Oslo). CFP-AR-YFP was transiently expressed in HeLa grown on standard 12 mm glass coverslips. Constructs were transfected using Lipofectamine 2000 (Invitrogen). Media was removed and replaced with fresh DMEM/F12 with 5% FBS 24 hr posttransfection. Cells were then treated overnight with compounds (20 hr) prepared in growth media (DMEM/F12, 5% FBS). Treatment was followed with these steps: fixation, 4% PFA (30 min); quench, 100 mM NH₄Cl (10 min); and mount with SlowFade Gold (Invitrogen). After fixation, cells were washed with PBS++ three times, while all other wash steps were performed with PIPES/HEPES/EGTA/MgCl₂ (PEM) buffer, prepared at a final pH of 6.8.

FRET imaging was performed as described previously with the DeltaVision Core Image Restoration Microscope (Applied Precision, Issaquah, WA, USA). Z-stacks were imaged at 0.2 μm separation and a frame size of 1,024 × 1,024 pixels at 1 × 1 binning with an Olympus IX71 microscope using a 60×, 1.42 NA Plan Achromat objective (Olympus, Center Valley, PA, USA), and a Photometrics CoolSnap HQ2 CCD camera. Filter sets were as follows, with a dichroic to split CFP and YFP: excitation 430 nm/emission 470 nm (CFP), excitation 500 nm/emission 535 nm (YFP), and excitation 430 nm/emission 535 nm (FRET). After deconvolution (Softworx, Applied Precision), FRET calculations were performed using the Applied Precision FRET user interface. FRET measurements on individual nuclei were acquired on maximum intensity projections of the derived FRET image. Spectral bleed through was corrected for by acquiring specimens containing only CFP-AR and YFP-AR. Standard values for α and β coefficients were 0.6 (CFP) and 0.12 (YFP) acquired from single donor/acceptor plasmid expression experiments. Additional and supporting analyses were performed using PixFRET (Feige et al., 2005).

AR NH₂-COOH Domain Interaction Assay

An interaction between COOH terminal AF2 (activation function 2) and NH₂ terminal sequence F²³XXLF²⁷ was measured using the CheckMate/Flexi Vector Mammalian Two-Hybrid System (Promega, Madison, WI, USA). A segment containing AR 1-660 was fused to the VP16 TAD domain of plasmid pFN10A, while segments AR 624-919 were fused to the Gal4-DBD domain of plasmid pFN11A. One day before transfection, 1.5 × 10⁶ HeLa cells were seeded into a 60-mm dish. Cells were cotransfected with 1.3 μg of pFN11A-AR624-919, 1.3 μg of pFN10A-1-660, 1.3 μg of pGL4.31 (containing five GAL4 binding sites upstream of a minimal TATA box, which is upstream of a firefly luciferase gene that acts as a reporter for interactions between proteins), and 1 ng of pRL-TK carrying the Renilla luciferase gene. After 12 hr of transfection, cells were trypsinized and equally seeded into a 96-well plate. Multireplicate detection of NH₂-COOH interaction was evaluated in ligand competition experiments where adipogenic compounds and OHF were titrated against 0.1 nM DHT. After 24 hr of treatment, luciferase activity was assayed with the Promega Dual Glo assay kit, using a luminometer (PerkinElmer). Data represent the units of firefly luciferase corrected for the units of renilla luciferase detected in the same plate. As controls to account for basal activity of pFN11A-AR624-919 and pFN10A-AR1-660, parallel experiments were performed with each plasmid expressed individually.

Luciferase Expression Experiments

We used replication deficient adenoviruses coupled with polylysine (Allgood et al., 1997) to express pARR₂PB-luciferase in human preadipocytes. Reporter gene activity was detected using the Promega Luciferase Assay Kit. Relative luminescence units were normalized to β-galactosidase activity using a standard 2-Nitrophenyl β-d-galactopyranoside (Sigma) colorimetric assay.

GFP-AR:ARR₂PB-dsRED2-skl Biosensor Experiments

We developed a stable cell line for cell-based HCA of AR translocation and reporter activity under treatment with adipogenic compounds. The parental GFP-AR HeLa cell line (Szafran et al., 2008) was infected with a lentivirus encoding a pARR₂PB-dsRED2skl reporter construct, based on the AR-responsive composite probasin promoter. This reporter encodes a dsRED2 protein (Clontech) fused at the C terminus with a peroxisome targeting sequence (SKL, serine, lysine, leucine) that serves to localize and concentrate the fluorescence signal. Antibiotic-resistant cultures were selected with both puromycin (1.5 μg/ml) and hygromycin (200 μg/ml) for 2 weeks. Subsequently, clones were single cell sorted by FACS where clones were identified based on GFP-AR and ARR₂PB-dsRED2-skl responsiveness (e.g., low GFP/high dsRED2). Single-cell clones in phenol-red-free DMEM (Mediatech) with 5% FBS, 100 U/ml penicillin, 100 μg/ml streptomycin, 1.5 μg/ml puromycin, and 200 μg/ml hygromycin. One single-cell clone (GFP-AR:ARR₂PB-dsRED2skl) that exhibited maximal DHT-responsive reporter activity was used for detecting androgenic effects of rosiglitazone, dexamethasone, insulin, IBMX, and OHF.

Before experiments, 384 well plates (Greiner Sensoplate Plus) were coated with FBS overnight. Cells were plated (4,000 cell/well), after excess FBS was removed from each well, using the TiterTek Multi-Drop Plus (TiterTek, Huntsville, AL, USA). GFP-AR:ARR₂PB-dsRED2skl cells were seeded in antibiotic-free, phenol-red-free DMEM containing 5% charcoal-stripped, dialyzed (SD) FBS and incubated 48 hr. Cells were then exposed to single doses of each compound in the presence or absence of 1 nM DHT. Vehicle (EtOH), 10 nM DHT, 10 μM OHF, and 1 nM DHT/10 μM OHF treatments functioned as controls, each in individual columns. After compound addition, cells were incubated 48 hr to allow for simultaneous detection of AR translocation and reporter expression. Plates were processed for imaging as previously described (Szafran et al., 2008).

Support Vector Machine Classification

For each experiment, a validation data set was created consisting of 16 wells for the following control treatments: vehicle (ethanol), agonist (10 nM DHT), a negative ligand control (10 μM OHF), and antagonist (10 μM OHF/1 nM DHT). After the image analysis and feature extraction steps described earlier, single-cell-level measurements were used to train a classifier on the control data set to distinguish between the control treatments. Before training, 1,000 single-cell samples were randomly sampled (without replacement) from each control treatment to ensure classes were equally sized in the training process. Next, linearly dependent features were removed. All other features were scaled to a range of [-1,1]. Feature selection was performed on the training data using stepwise discriminant analysis (SDA), which defines a list of the most discriminative feature for classification (Jenrich, 1977). Finally, we used the SDA-selected features to train a support vector machine (SVM) classifier with a radial-basis-function kernel (Cortes and Vapnik, 1995). Tenfold cross-validation on the training data was used with a grid search to optimize the parameters C (slack penalty) and g (kernel parameter).

For validation, we randomly sampled 10 different sets upon which we trained a classifier, and for each corresponding subtraining set, we tested its classifier on the remaining control samples. Resulting classification labels were used to calculate precision and recall scores for each classifier, and these accuracy metrics were averaged across the panel of classifiers to produce a performance measure for the classification approach. The supervised learning approach was implemented in Python 2.6 and utilizes LIBSVM 2.9 (<http://www.csie.ntu.edu.tw/~cjlin/libsvm/>).

Statistical Analyses

Data presented were acquired from a minimum of two (quantitative real-time PCR) or three (HCA) independent experiments performed on multiple days, unless otherwise indicated. ANOVA was first used to compare the effects of

time or ligand treatment. If significant differences were identified, then data were compared with Tukey's honestly significant difference post hoc tests. All tests were carried out at the 95% confidence interval using JMP-IN 7 (SAS, Cary, NC, USA).

ACCESSION NUMBERS

The Gene Expression Omnibus (GEO) accession number for the microarray data reported in this article is GSE39342.

SUPPLEMENTAL INFORMATION

Supplemental Information includes one figure, one Excel file, and one table and can be found with this article online at <http://dx.doi.org/10.1016/j.chembiol.2012.07.020>.

ACKNOWLEDGMENTS

This work was funded by National Institutes of Health (NIH) Grant 5R01DK055622, the Hankamer Foundation, and the U.S. Department of Defense Prostate Cancer Research Program (DAMD W81XWH-10-1-0390), with pilot grant and equipment support from the John S. Dunn Gulf Coast Consortium for Chemical Genomics (M.A.M.). Additional funding was provided by NIH Grants 1F32DK85979 (S.M.H.), 5T32HD007165 (to B.W. O'Malley), 5K01DK081446 (B.H.), 5K12DK083014 (to D.J. Lamb), 3U19DK062434 (Nuclear Receptor Signaling Atlas), and the Caroline Weiss Law Foundation (S.E.M.). Imaging resources were supported by NIH Grants SCCPR U54 HD-007495 (to F.J. DeMayo), P30 DK-56338 (to M.K. Estes), P30 CA-125123 (to C.K. Osborne), and the Dan L. Duncan Cancer Center of Baylor College of Medicine. The authors thank Huiying Sun, Maureen G. Mancini, Leoncio Vergara, and Jim Broughman for technical resource support. The authors also thank Nancy Weigel and Fabio Stossi for critical review of the manuscript. B.B. is an employee of Zen Bio, Inc.

Received: March 19, 2012

Revised: July 5, 2012

Accepted: July 9, 2012

Published: September 20, 2012

REFERENCES

- Allgood, V.E., Zhang, Y., O'Malley, B.W., and Weigel, N.L. (1997). Analysis of chicken progesterone receptor function and phosphorylation using an adenovirus-mediated procedure for high-efficiency DNA transfer. *Biochemistry* **36**, 224–232.
- Archer, T.K., Lee, H.L., Cordingley, M.G., Mymryk, J.S., Fragoso, G., Berard, D.S., and Hager, G.L. (1994). Differential steroid hormone induction of transcription from the mouse mammary tumor virus promoter. *Mol. Endocrinol.* **8**, 568–576.
- Ashcroft, F.J., Newberg, J.Y., Jones, E.D., Mikic, I., and Mancini, M.A. (2011). High content imaging-based assay to classify estrogen receptor- α ligands based on defined mechanistic outcomes. *Gene* **477**, 42–52.
- Blouin, K., Nadeau, J., Mailloux, M., Daris, S., Lebel, L.-T., Van, and Tchernof, A. (2009a). Pathways of adipose tissue androgen metabolism in women: depot differences and modulation by adipogenesis. *Am J. Physiol. Endocrinol. Metab.* **296**, E244–E255.
- Blouin, K., Veilleux, A., Luu-The, V., and Tchernof, A. (2009b). Androgen metabolism in adipose tissue: recent advances. *Mol. Cell. Endocrinol.* **307**, 97–103.
- Blouin, K., Nadeau, M., Perreault, M., Veilleux, A., Drolet, R., Marceau, P., Mailloux, J., Luu-The, V., and Tchernof, A. (2010). Effects of androgens on adipocyte differentiation and adipose tissue explant metabolism in men and women. *Clin. Endocrinol. (Oxf.)* **72**, 176–188.
- Bolton, E.C., So, A.Y., Chaivorapol, C., Haqq, C.M., Li, H., and Yamamoto, K.R. (2007). Cell- and gene-specific regulation of primary target genes by the androgen receptor. *Genes Dev.* **21**, 2005–2017.
- Bujalska, I.J., Quinkler, M., Tomlinson, J.W., Montague, C.T., Smith, D.M., and Stewart, P.M. (2006). Expression profiling of 11 β -hydroxysteroid dehydrogenase type-1 and glucocorticoid-target genes in subcutaneous and omental human preadipocytes. *J. Mol. Endocrinol.* **37**, 327–340.
- Burnstein, K.L., Maiorino, C.A., Dai, J.L., and Cameron, D.J. (1995). Androgen and glucocorticoid regulation of androgen receptor cDNA expression. *Mol. Cell Endocrinol.* **115**, 177–186.
- Chambon, C., Duteil, D., Vignaud, A., Ferry, A., Messaddeq, N., Malivindi, R., Kato, S., Chambon, P., and Metzger, D. (2010). Myocytic androgen receptor controls the strength but not the mass of limb muscles. *Proc. Natl. Acad. Sci. USA* **107**, 14327–14332.
- Chang, C.S., Kokontis, J., and Liao, S.T. (1988). Molecular cloning of human and rat complementary DNA encoding androgen receptors. *Science* **240**, 324–326.
- Chen, S.Y., Wang, J., Yu, G.Q., Liu, W.H., and Pearce, D. (1997). Androgen and glucocorticoid receptor heterodimer formation - A possible mechanism for mutual inhibition of transcriptional activity. *J. Biol. Chem.* **272**, 14087–14092.
- Cortes, C., and Vapnik, V. (1995). Support vector networks. *Mach. Learn.* **20**, 273–297.
- Coviello, A.D., Legro, R.S., and Dunaif, A. (2006). Adolescent girls with polycystic ovary syndrome have an increased risk of the metabolic syndrome associated with increasing androgen levels independent of obesity and insulin resistance. *J. Clin. Endocrinol. Metab.* **91**, 492–497.
- Dati, E., Baroncelli, G.I., Mora, S., Russo, G., Baldinotti, F., Parrini, D., Erba, P., Simi, P., and Bertelloni, S. (2009). Body composition and metabolic profile in women with complete androgen insensitivity syndrome. *Sex Dev.* **3**, 188–193.
- Davies, P., and Rushmere, N.K. (1990). Association of glucocorticoid receptors with prostate nuclear sites for androgen receptors and with androgen response elements. *J. Mol. Endocrinol.* **5**, 117–127.
- De Vos, P., Lefebvre, A.M., Miller, S.G., Guerre-Millo, M., Wong, K., Saladin, R., Hamann, L.G., Staels, B., Briggs, M.R., and Auwerx, J. (1996). Thiazolidinediones repress ob gene expression in rodents via activation of peroxisome proliferator-activated receptor gamma. *J. Clin. Invest.* **98**, 1004–1009.
- Feige, J.N., Sage, D., Wahli, W., Desvergne, B., and Gelman, L. (2005). PixFRET, an ImageJ plug-in for FRET calculation that can accommodate variations in spectral bleed-throughs. *Microsc. Res. Tech.* **68**, 51–58.
- Fu, M., Sun, T., Bookout, A.L., Downes, M., Yu, R.T., Evans, R.M., and Mangelsdorf, D.J. (2005). A nuclear receptor atlas: 3T3-L1 adipogenesis. *Mol. Endocrinol.* **19**, 2437–2450.
- Fujikura, J., Fujimoto, M., Yasue, S., Noguchi, M., Masuzaki, H., Hosoda, K., Tachibana, T., Sugihara, H., and Nakao, K. (2005). Insulin-induced lipohypertrophy: Report of a case with histopathology. *Endocr. J.* **52**, 623–628.
- Furutani, T., Watanabe, T., Tanimoto, K., Hashimoto, T., Koutoku, H., Kudoh, M., Shimizu, Y., Kato, S., and Shikama, H. (2002). Stabilization of androgen receptor protein is induced by agonist, not by antagonists. *Biochem. Biophys. Res. Commun.* **294**, 779–784.
- Gould, D.C., Kirby, R.S., and Amoroso, P. (2007). Hypoandrogen-metabolic syndrome: a potentially common and underdiagnosed condition in men. *Int. J. Clin. Pract.* **61**, 341–344.
- Guilherme, A., Virbasius, J.V., Puri, V., and Czech, M.P. (2008). Adipocyte dysfunctions linking obesity to insulin resistance and type 2 diabetes. *Nat. Rev. Mol. Cell Biol.* **9**, 367–377.
- Gupta, V., Bhasin, S., Guo, W., Singh, R., Miki, R., Chauhan, P., Choong, K., Tchkonja, T., Lebrasseur, N.K., Flanagan, J.N., Hamilton, J.A., Viereck, J.C., Narula, N.S., Kirkland, J.L., and Jasuja, R. (2008). Effects of dihydrotestosterone on differentiation and proliferation of human mesenchymal stem cells and preadipocytes. *Mol. Cell Endocrinol.* **296**, 32–40.
- Hartig, S.M., He, B., Long, W., Buehrer, B.M., and Mancini, M.A. (2011). Homeostatic levels of SRC-2 and SRC-3 promote early human adipogenesis. *J. Cell Biol.* **192**, 55–72.
- Hotamisligil, G.S., Johnson, R.S., Distel, R.J., Ellis, R., Papaioannou, V.E., and Spiegelman, B.M. (1996). Uncoupling of obesity from insulin resistance

- through a targeted mutation in aP2, the adipocyte fatty acid binding protein. *Science* 274, 1377–1379.
- Jennrich, R.I. (1977). Stepwise discriminant analysis. In *Statistical methods for digital computers*, K. Enslein, A. Ralston, and H.S. Wilf, eds. (New York, NY: John Wiley & Sons), pp. 77–95.
- Jones, J.O., An, W.F., and Diamond, M.I. (2009). AR inhibitors identified by high-throughput microscopy detection of conformational change and subcellular localization. *ACS Chem. Biol.* 4, 199–208.
- Kempainen, J.A., Langley, E., Wong, C.I., Bobseine, K., Kelce, W.R., and Wilson, E.M. (1999). Distinguishing androgen receptor agonists and antagonists: distinct mechanisms of activation by medroxyprogesterone acetate and dihydrotestosterone. *Mol. Endocrinol.* 13, 440–454.
- Klokk, T.I., Kurys, P., Elbi, C., Nagaich, A.K., Hendarwanto, A., Slagsvold, T., Chang, C.Y., Hager, G.L., and Saatcioglu, F. (2007). Ligand-specific dynamics of the androgen receptor at its response element in living cells. *Mol. Cell Biol.* 27, 1823–1843.
- Lahnalampi, M., Heinäniemi, M., Sinkkonen, L., Wabitsch, M., and Carlberg, C. (2010). Time-resolved expression profiling of the nuclear receptor superfamily in human adipogenesis. *PLoS ONE* 5, e12991.
- Langley, E., Zhou, Z.X., and Wilson, E.M. (1995). Evidence for an anti-parallel orientation of the ligand-activated human androgen receptor dimer. *J. Biol. Chem.* 270, 29983–29990.
- Lee, M.J., Fried, S.K., Mundt, S.S., Wang, Y., Sullivan, S., Stefanni, A., Daugherty, B.L., and Hermanowski-Vosatka, A. (2008). Depot-specific regulation of the conversion of cortisone to cortisol in human adipose tissue. *Obesity (Silver Spring)* 16, 1178–1185.
- Lieberman, B.A., Bona, B.J., Edwards, D.P., and Nordeen, S.K. (1993). The constitution of a progesterone response element. *Mol. Endocrinol.* 7, 515–527.
- Liu, J., and Farmer, S.R. (2004). Regulating the balance between peroxisome proliferator-activated receptor gamma and beta-catenin signaling during adipogenesis. A glycogen synthase kinase 3beta phosphorylation-defective mutant of beta-catenin inhibits expression of a subset of adipogenic genes. *J. Biol. Chem.* 279, 45020–45027.
- Liu, S., Navarro, G., and Mauvais-Jarvis, F. (2010). Androgen excess produces systemic oxidative stress and predisposes to beta-cell failure in female mice. *PLoS ONE* 5, e11302.
- Lombès, M., Binart, N., Oblin, M.E., Joulin, V., and Baulieu, E.E. (1993). Characterization of the interaction of the human mineralocorticosteroid receptor with hormone response elements. *Biochem. J.* 292, 577–583.
- Lubahn, D.B., Joseph, D.R., Sullivan, P.M., Willard, H.F., French, F.S., and Wilson, E.M. (1988). Cloning of human androgen receptor complementary DNA and localization to the X chromosome. *Science* 240, 327–330.
- Madsen, L., Pedersen, L.M., Liaset, B., Ma, T., Petersen, R.K., van den Berg, S., Pan, J., Muller-Decker, K., Dulsner, E.D., Kleemann, R., Kooistra, T., Dorskeland, S.O., and Kristiansen, K. (2008). cAMP-dependent signaling regulates the adipogenic effect of n-6 polyunsaturated fatty acids. *J. Biol. Chem.* 283, 7196–7205.
- Magee, J.A., Chang, L.W., Stormo, G.D., and Milbrandt, J. (2006). Direct, androgen receptor-mediated regulation of the FKBP5 gene via a distal enhancer element. *Endocrinology* 147, 590–598.
- Massie, C.E., Lynch, A., Ramos-Montoya, A., Boren, J., Stark, R., Fazli, L., Warren, A., Scott, H., Madhu, B., Sharma, N., et al. (2011). The androgen receptor fuels prostate cancer by regulating central metabolism and biosynthesis. *EMBO J.* 30, 2719–2733.
- Masuzaki, H., Paterson, J., Shinyama, H., Morton, N.M., Mullins, J.J., Seckl, J.R., and Flier, J.S. (2001). A transgenic model of visceral obesity and the metabolic syndrome. *Science* 294, 2166–2170.
- Masuzaki, H., Yamamoto, H., Kenyon, C.J., Elmquist, J.K., Morton, N.M., Paterson, J.M., Shinyama, H., Sharp, M.G.F., Fleming, S., Mullins, J.J., Seckl, J.R., and Flier, J.S. (2003). Transgenic amplification of glucocorticoid action in adipose tissue causes high blood pressure in mice. *J. Clin. Invest.* 112, 83–90.
- Mikkelsen, T.S., Xu, Z., Zhang, X., Wang, L., Gimble, J.M., Lander, E.S., and Rosen, E.D. (2010). Comparative epigenomic analysis of murine and human adipogenesis. *Cell* 143, 156–169.
- Moss, P.E., Lyles, B.E., and Stewart, L.V. (2010). The PPAR gamma ligand ciglitazone regulates androgen receptor activation differently in androgen-dependent versus androgen-independent human prostate cancer cells. *Exp. Cell Res.* 316, 3478–3488.
- Nazareth, L.V., Stenoien, D.L., Bingman, W.E., 3rd, James, A.J., Wu, C., Zhang, Y., Edwards, D.P., Mancini, M., Marcelli, M., Lamb, D.J., and Weigel, N.L. (1999). A C619Y mutation in the human androgen receptor causes inactivation and mislocalization of the receptor with concomitant sequestration of SRC-1 (steroid receptor coactivator 1). *Mol. Endocrinol.* 13, 2065–2075.
- Nishino, N., Tamori, Y., Tateya, S., Kawaguchi, T., Shibakusa, T., Mizunoya, W., Inoue, K., Kitazawa, R., Kitazawa, S., Matsuki, Y., et al. (2008). FSP27 contributes to efficient energy storage in murine white adipocytes by promoting the formation of unilocular lipid droplets. *J. Clin. Invest.* 118, 2808–2821.
- Nordeen, S.K., Suh, B.J., Kühnel, B., and Hutchison, C.A., 3rd. (1990). Structural determinants of a glucocorticoid receptor recognition element. *Mol. Endocrinol.* 4, 1866–1873.
- Pantoja, C., Huff, J.T., and Yamamoto, K.R. (2008). Glucocorticoid signaling defines a novel commitment state during adipogenesis in vitro. *Mol. Biol. Cell* 19, 4032–4041.
- Rary, C.M., Ratcliffe, S.J., Weinstein, R., Bhasin, S., Blackman, M.R., Cauley, J.A., Robbins, J., Zmuda, J.M., Harris, T.B., and Cappola, A.R. (2011). Higher serum free testosterone concentration in older women is associated with greater bone mineral density, lean body mass, and total fat mass: the cardiovascular health study. *J. Clin. Endocrinol. Metab.* 96, 989–996.
- Reddy, T.E., Pauli, F., Sprouse, R.O., Neff, N.F., Newberry, K.M., Garabedian, M.J., and Myers, R.M. (2009). Genomic determination of the glucocorticoid response reveals unexpected mechanisms of gene regulation. *Genome Res.* 19, 2163–2171.
- Roche, P.J., Hoare, S.A., and Parker, M.G. (1992). A consensus DNA-binding site for the androgen receptor. *Mol. Endocrinol.* 6, 2229–2235.
- Rosen, E.D., Sarraf, P., Troy, A.E., Bradwin, G., Moore, K., Milstone, D.S., Spiegelman, B.M., and Mortensen, R.M. (1999). PPAR gamma is required for the differentiation of adipose tissue in vivo and in vitro. *Mol. Cell* 4, 611–617.
- Rosen, E.D., Hsu, C.H., Wang, X.Z., Sakai, S., Freeman, M.W., Gonzalez, F.J., and Spiegelman, B.M. (2002). C/EBP alpha induces adipogenesis through PPAR gamma: a unified pathway. *Genes Dev.* 16, 22–26.
- Schaufele, F., Carbonell, X., Guerbadot, M., Borngräber, S., Chapman, M.S., Ma, A.A.K., Miner, J.N., and Diamond, M.I. (2005). The structural basis of androgen receptor activation: Intramolecular and intermolecular amino-carboxy interactions. *Proc. Natl. Acad. Sci. USA* 102, 9802–9807.
- Schoenmakers, E., Verrijdt, G., Peeters, B., Verhoeven, G., Rombauts, W., and Claessens, F. (2000). Differences in DNA binding characteristics of the androgen and glucocorticoid receptors can determine hormone-specific responses. *J. Biol. Chem.* 275, 12290–12297.
- Schupp, M., Cristancho, A.G., Lefterova, M.I., Hanniman, E.A., Briggs, E.R., Steger, D.J., Qatanani, M., Curtin, J.C., Schug, J., Ochsner, S.A., McKenna, N.J., and Lazar, M.A. (2009). Re-expression of GATA2 Cooperates with Peroxisome Proliferator-activated Receptor-gamma Depletion to Revert the Adipocyte Phenotype. *J. Biol. Chem.* 284, 9458–9464.
- Singh, R., Artaza, J.N., Taylor, W.E., Gonzalez-Cadavid, N.F., and Bhasin, S. (2003). Androgens stimulate myogenic differentiation and inhibit adipogenesis in C3H 10T1/2 pluripotent cells through an androgen receptor-mediated pathway. *Endocrinology* 144, 5081–5088.
- Singh, R., Artaza, J.N., Taylor, W.E., Braga, M., Yuan, X., Gonzalez-Cadavid, N.F., and Bhasin, S. (2006). Testosterone inhibits adipogenic differentiation in 3T3-L1 cells: Nuclear translocation of androgen receptor complex with beta-catenin and T-cell factor 4 may bypass canonical Wnt signaling to down-regulate adipogenic transcription factors. *Endocrinology* 147, 141–154.

- Soccio, R.E., Tuteja, G., Everett, L.J., Li, Z., Lazar, M.A., and Kaestner, K.H. (2011). Species-specific strategies underlying conserved functions of metabolic transcription factors. *Mol. Endocrinol.* *25*, 694–706.
- Stanworth, R.D., and Jones, T.H. (2009). Testosterone in obesity, metabolic syndrome and Type 2 diabetes. In *Advances in the Management of Testosterone Deficiency, Vol. 37*, T.H. Jones, ed. (Basel, Switzerland: Karger), pp. 74–90.
- Steger, D.J., Grant, G.R., Schupp, M., Tomaru, T., Lefterova, M.I., Schug, J., Manduchi, E., Stoeckert, C.J., and Lazar, M.A. (2010). Propagation of adipogenic signals through an epigenomic transition state. *Genes Dev.* *24*, 1035–1044.
- Szafran, A.T., Szwarc, M., Marcelli, M., and Mancini, M.A. (2008). Androgen receptor functional analyses by high throughput imaging: determination of ligand, cell cycle, and mutation-specific effects. *PLoS ONE* *3*, e3605.
- Tenover, J.S. (1992). Effects of testosterone supplementation in the aging male. *J. Clin. Endocrinol. Metab.* *75*, 1092–1098.
- Tontonoz, P., Hu, E., and Spiegelman, B.M. (1994). Stimulation of adipogenesis in fibroblasts by PPAR gamma 2, a lipid-activated transcription factor. *Cell* *79*, 1147–1156.
- Veilleux, A., Côté, J.A., Blouin, K., Nadeau, M., Pelletier, M., Marceau, P., Laberge, P.Y., Luu-The, V., and Tchernof, A. (2012). Glucocorticoid-induced androgen inactivation by aldo-keto reductase 1C2 promotes adipogenesis in human preadipocytes. *Am. J. Physiol. Endocrinol. Metab.* *302*, E941–E949.
- Wake, D.J., Strand, M., Rask, E., Westerbacka, J., Livingstone, D.E.W., Soderberg, S., Andrew, R., Yki-Jarvinen, H., Olsson, T., and Walker, B.R. (2007). Intra-adipose sex steroid metabolism and body fat distribution in idiopathic human obesity. *Clin. Endocrinol. (Oxf.)* *66*, 440–446.
- Waki, H., Park, K.W., Mitro, N., Pei, L., Damoiseaux, R., Wilpitz, D.C., Reue, K., Saez, E., and Tontonoz, P. (2007). The small molecule harmine is an antidiabetic cell-type-specific regulator of PPARgamma expression. *Cell Metab.* *5*, 357–370.
- Wallace, A.D., and Cidlowski, J.A. (2001). Proteasome-mediated glucocorticoid receptor degradation restricts transcriptional signaling by glucocorticoids. *J. Biol. Chem.* *276*, 42714–42721.
- Wilson, E.M., and French, F.S. (1976). Binding properties of androgen receptors. Evidence for identical receptors in rat testis, epididymis, and prostate. *J. Biol. Chem.* *251*, 5620–5629.
- Yang, C.C., Ku, C.Y., Wei, S., Shiau, C.W., Chen, C.S., Pinzone, J.J., and Ringel, M.D. (2006). Peroxisome proliferator-activated receptor gamma-independent repression of prostate-specific antigen expression by thiazolidinediones in prostate cancer cells. *Mol. Pharmacol.* *69*, 1564–1570.
- Yen, P.M., Liu, Y., Palvimo, J.J., Trifiro, M., Whang, J., Pinsky, L., Janne, O.A., and Chin, W.W. (1997). Mutant and wild-type androgen receptors exhibit cross-talk on androgen-, glucocorticoid-, and progesterone-mediated transcription. *Mol. Endocrinol.* *11*, 162–171.
- Yu, C.Y., Mayba, O., Lee, J.V., Tran, J., Harris, C., Speed, T.P., and Wang, J.C. (2010). Genome-wide analysis of glucocorticoid receptor binding regions in adipocytes reveal gene network involved in triglyceride homeostasis. *PLoS ONE* *5*, e15188.
- Zitzmann, M. (2009). Testosterone deficiency, insulin resistance and the metabolic syndrome. *Nat. Rev. Endocrinol.* *5*, 673–681.